Pure Appl. Geophys.

https://doi.org/10.1007/s00024-019-02372-4

Pure and Applied Geophysics

Probabilistic Tsunami Hazard Assessment for Local and Regional Seismic Sources Along the Pacific Coast of Central America with Emphasis on the Role of Selected Uncertainties

Natalia Zamora[1,2] and Andrey Y. Babeyko[3]

Abstract—Historical data indicate that the Middle America subduction zone represents the primary tsunamigenic source that affects the Central American coastal areas. In recent years, the tsunami potential in the region has mainly been assessed using maximum credible earthquakes or historical events showing moderate tsunami potential. However, such deterministic scenarios are not provided with their adequate probability of occurrence. In this study, earthquake rates have been combined with tsunami numerical modeling in order to assess probabilistic tsunami hazard posed by local and regional seismic sources. The common conceptual framework for the probabilistic seismic hazard assessment has been adapted to estimate the probabilities of exceeding certain tsunami amplitudes along the Central American Pacific coast. The study area encompasses seismic sources related to the Central America, Colombia and Ecuador subduction zones. In addition to the classical subduction inter-plate events, this study also incorporates sources at the outer rise, within the Caribbean crust as well as intra-slab sources. The study yields conclusive remarks showing that the highest hazard is posed to northwestern Costa Rica, El Salvador and the Nicaraguan coast, southern Colombia and northern Ecuador. In most of the region it is 50 to 80% likely that the tsunami heights will exceed 2 m for the 500 year time exposure (T). The lowest hazard appears to be in the inner part of the Fonseca Gulf, Honduras. We also show the large dependence of PTHA on model assumptions. While the approach taken in this study represents a thorough step forward in tsunami hazard assessment in the region, we also highlight that the integration of all possible uncertainties will be necessary to generate rigorous hazard models required for risk planning.

Keywords: Seismic segmentation, earthquake rates, tsunami hazard, Central America, Colombia, Ecuador, subduction zones.

1. Introduction

There is an increasing awareness of tsunami threat worldwide and a need for preparing for these infrequent yet destructive events. Lately, more concern has arisen in regions like Central America where probabilities of large tsunamis are uncertain. Central America (CAM) lies in a region of high seismic rates where moderate to large earthquakes are common, and at least forty tsunamis (Fig. 1) have reached the coastal regions in the last 500 years (NGDC/WDS 2017). The likelihood of mega-earthquakes along CAM is unclear (Ye et al. 2013), although moderate earthquakes such as the 'tsunami earthquakes' caused by slow ruptures have triggered large tsunamis despite their moderate seismic moment (Kanamori 1972; Satake 1994; Borrero et al. 2014). The latter has raised interest in assessing the tsunamigenic potential of local sources by using different methods to account for the hazard in the region (Zamora and Babeyko 2015; Parsons and Geist 2009a).

There are two main approaches to estimating tsunami hazard. The most common approach is known as scenario-based, where numerical simulations are performed with credible worst-case scenarios (Lorito et al. 2008; Løvholt et al. 2012). Those scenarios are either designed by assuming synthetic events similar to historical ones, or are based on geological constraints to estimate maximum credible earthquake scenarios (MCE). Most of the tsunami studies in the CAM region have assessed tsunami threat using the scenario-based approach. Hence, in this approach neither the return periods of tsunamis, their probabilities of occurrence, nor their plausibility have been estimated. The second approach, called the Probabilistic Tsunami Hazard Assessment (PTHA),

Electronic supplementary material The online version of this article (https://doi.org/10.1007/s00024-019-02372-4) contains supplementary material, which is available to authorized users.

[1] Research Center for Integrated Disaster Risk Management (CIGIDEN), CONICYT/FONDAP/15110017, Santiago, Chile. E-mail: natalia.zamora@cigiden.cl

[2] CYCLO Millennium Nucleus The Seismic Cycle Along Subduction Zones, Valdivia, Chile.

[3] GFZ German Research Centre for Geosciences, Telegrafenberg, 14473 Potsdam, Germany.

Published online: 28 November 2019

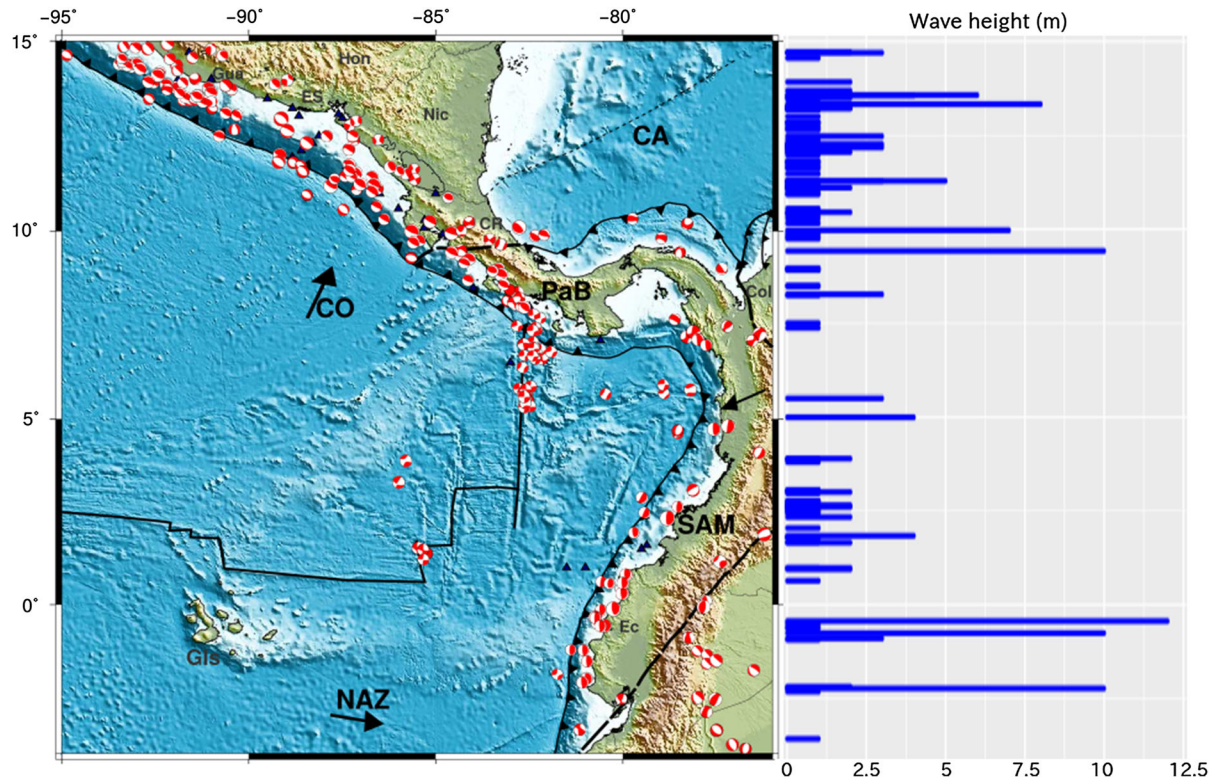

Figure 1
Tectonic setting of study area (left) and bar plot showing tsunami wave heights registered along the Pacific coast of Central America since 1900 (right). Runup data from Mexico to Ecuador are based on the National Geophysical Data Center (NGDC/WDS 2017) that covers a time of 500 years in this region. Note that some tsunami events that appear in the NGDC catalog do not have runup or wave height data but only limited information such as the year of occurrence

has become a necessary framework for dealing with multiple sources and accounting for their uncertainties (Grezio et al. 2017).

PTHA was established following procedures similar to those used for probabilistic seismic hazard assessment (Cornell 1968; McGuire 1976). The purpose of the seismic PTHA is to assess all possible earthquake sources that may contribute to the tsunami hazard and to statistically evaluate their corresponding tsunami impact in a probabilistic sense. PTHA results can be then used in risk assessment (Løvholt et al. 2012; Schaefer et al. 2015). For this, tsunami sources (e.g. earthquakes) and their probabilistic recurrence models are integrated with numerical simulations of tsunami propagation, or, alternatively, with empirical relationships between magnitude and wave runup to find tsunami rates of occurrence and return periods, as the probabilities of exceedance of wave height thresholds at particular coastal sites (Burroughs and Tebbens 2005; Geist and Parsons 2006; Thio et al. 2007; Sørensen et al. 2012). In addition to the seismically triggered tsunamis, PTHA has been also applied to other tsunami sources such as submarine landslides (Ward 2001) and asteroid impacts (Ward and Asphaug 2000).

The availability of tsunami runup records in tsunami catalogs for CAM might not be sufficient to make confident hazard estimates with only empirical relationships between earthquake parameters and local runup. To our knowledge, only two studies in Central America assess tsunami hazard in an empirical way. One covers the entire Caribbean basin (Parsons and Geist 2009a), while the other assessed tsunami hazard along the Pacific coast of Central America, taking into account hybrid methods by combining probability of earthquake occurrence and

empirical relations to get tsunami amplitudes from Mexico to Ecuador (Brizuela et al. 2014). At the national level, some reports have been prepared under the Central American Probabilistic Risk Assessment (CAPRA) program (http://www.ecapra.org), nonetheless these models have not considered the associated uncertainties in the tsunami hazard modeling.

Therefore, while only two studies exist that provide probabilistic hazard estimates, most of the tsunami hazard research for this region has used a scenario-based deterministic approach (Zamora and Babeyko 2015; Fernández et al. 2004; Ortiz et al. 2001; Álvarez-Gómez et al. 2013). These studies considered historical scenarios to simulate tsunami threat to specific regions of Central America, for instance, El Salvador or the Puntarenas port, Costa Rica, and could provide a significant inputs for evacuation maps. Despite the large uncertainties drawn in PTHA, this approach is important since it allows to quantify probabilities of occurrence which are needed in many aspects of coastal risk planning.

The aim of this study is to assess the probability of exceedance of certain wave heights (tsunamis) along the Pacific coast of Central America by integrating local and regional tectonic sources along the Pacific coast from Guatemala to Ecuador, also highlighting the dependency of hazard estimates on model assumptions. The Monte Carlo technique has been implemented to account for seismic source uncertainties. Our study is based on a similar approach to the well-known PSHA in which the whole source region is divided into several seismo-tectonic zones characterized with constant seismic patterns (Cornell 1968).

The seismo-tectonic segmentation model is a crucial assumption for this PTHA. Several sources of information have been integrated to assess the possible asperities that could show different seismic patterns that allow to separate the region into seismo-tectonic segments. One of these constraints is the fact that strong seismic coupling is unevenly distributed, and mainly low coupling prevails along the Central America convergent margin (Alvarado et al. 2010; Álvarez-Gómez et al. 2008; Correa-Mora et al. 2009; Lyon-Caen et al. 2006; Kobayashi et al. 2014; LaFemina et al. 2009) which might partly explain the unlikely occurrence of megathrust earthquakes (Ye et al. 2013). The geodetic studies, and the geological and geomorphic imprints along Central America lead to a regional seismo-tectonic model (Alvarado et al. 2017) that has been adapted in this study to assess the tsunami hazard posed from the outer rise, inter-plate, intra-slab and crustal seismicity.

Alternatively, to explore the limits of PTHA uncertainty in regard to zonation models, we include hazard estimates that resulted from the premise that the CAM megathrust could rupture up to Mw 9.0 without any segmentation along strike (McCaffrey 2008). Another factor of PTHA uncertainty that we would like to test in our study is a concept of depth-dependent crustal rigidity (Bilek and Lay, 1999) which is believed to be a potential cause for the so-called 'tsunami earthquakes' (Kanamori 1972) known to occur in the Central American region.

2. *Methods: Steps in PTHA and Input Data*

The probabilistic tsunami hazard is assessed here by combining the seismic source rates with tsunami numerical modeling. The seismic source recurrence rate is used to sample magnitudes (Mi) from the Gutenberg-Richter type magnitude-frequency distribution with Monte Carlo techniques. The latter is an efficient tool to account for randomness of seismic occurrence as well as the fault characterization.

The method used in this study follows a similar approach as previous studies that assess the seismic hazard (Wiemer et al. 2008) and the tsunami hazard (Geist 2009; Sørensen et al. 2012). The first step is to determine earthquake or seismo-tectonic source zones and to estimate their statistical seismic parameters. This so called zone-based approach has also been the frame in regional probabilistic seismic hazard assessment in the region (Benito et al. 2012; Salazar et al. 2013). A sketch illustrating our approach is provided in Fig. 2.

2.1. *Regional Seismic Catalogs*

The regional seismic catalog (herein, CAT2011) resulted from an extensive compilation of several historical earthquakes and national catalogs (Rojas

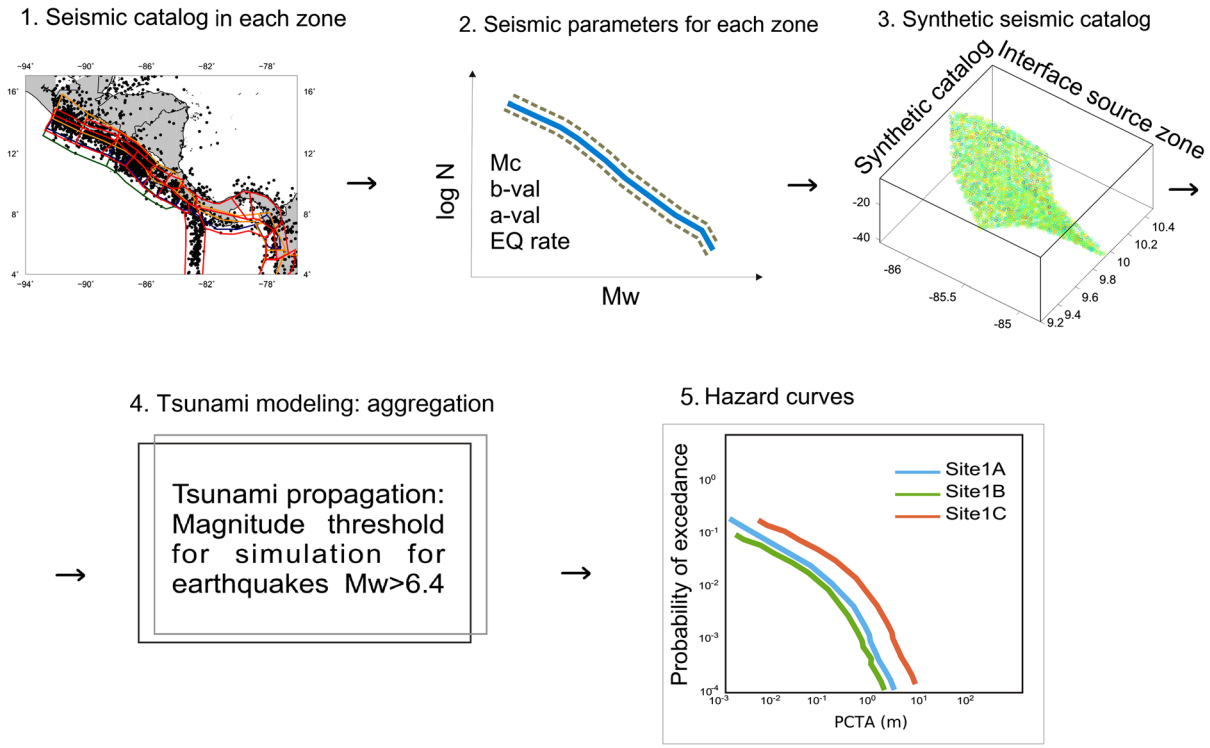

Figure 2
Schema that shows the steps of the probabilistic tsunami hazard assessment (PTHA) used in this study. *PCTA* peak coastal tsunami amplitudes

et al. 2013). The seismic databases of each country were homogenized with moment magnitude Mw using various empirical relationships, some of them defined for a specific country. In case of Panama, all events had Mw already calculated (Alvarado et al. 2017). Central American earthquake hypocenters have been collected through the Central America Seismological Center (CASC) since 1991. The CASC database is a complement to the global earthquake data since it covers earthquakes down to smaller magnitudes (Lindholm et al. 2004). The CASC was an initiative funded by the Norwegian Agency for International Cooperation, through the Center for the Prevention of Natural Disaster in Central America, and was created to improve national seismological networks and data exchange within Central American countries that could aid seismic zonation and hazard analysis among others.

CAT2011 has been generated in three main updating steps. The basis of this regional catalog was first described in Rojas et al. (1993), then updated during the RESISII project for the year 2007. Data of the Central American Seismological Centre (CASC) and the national catalogs have been integrated. CAT2011 has been updated until June 2011 as an integrated effort between the Central America national entities and the Polytechnic University of Madrid. Currently, it includes events starting from 1522. An extensive revision of the data and homogenization of magnitudes into Mw for all events of Mw $>$ 3.5 has been conducted by W. Rojas (persCom).

The CASC had contributed until 2011 as a continuous effort of the national seismological centers to assess seismicity patterns and to estimate seismic hazard. Constant improvements have been done to create a regional seismic catalog (Lindholm et al. 2004; Benito et al. 2012; Alvarado et al. 2017; Rojas et al. 1993). The 2011 catalog (CAT2011) initially contained about 55250 events, which was reduced to about 23000 earthquakes with magnitudes $>$ Mw 3.5 after using the de-clustering method proposed by Knopoff et al. (1982),

Additionally, for this study we obtained Colombian seismicity from the Comcat composite catalog (USGS 2017) by selecting earthquakes above Mw 4. For Ecuador, we employed the seismic catalog used in Beauval et al. (2013), which accounts for a minimum magnitude of Mw 3.5. For the entire catalog we also add information from different local studies.

We also retrieved the focal mechanisms from the GCMT website (Ekström et al. 2012) to get the main characterizations of the different tectonic regimes. This information was used to generate synthetic catalogs, as will be described later. A total of 2584 events for the period 1934–2013 have focal mechanism information, covering the geographic window delimited by the coordinates Lon 100° W–82° W and Lat 4° N–17° N, including the moment magnitudes above Mw 4.5.

2.2. *Seismo-Tectonic Zonation*

In this study, a zonation-based approach has been carried out, which means that geological and geomorphic imprints as well as geodetic and seismological characterization has been considered to differentiate segments in a similar way as in previous tsunami hazard assessment in other regions (Matias et al. 2013; Basili et al. 2013). It is assumed that within each seismic source zone, seismicity rates are constant and their parameters can be assessed by fitting the Gutenberg-Richter distribution (Cornell 1968).

The seismo-tectonic zonation model for Central America, Colombia and Ecuador (CAM-CE) is presented in Fig. 3. This model includes separate zones regarding their typical fault mechanisms which is not always undertaken in PSHA (e.g. Benito et al. 2012). Following Alvarado et al. (2017), we implemented a modified model that integrates such available data adapted for the PTHA (Zamora 2016). Particularly, several considerations are taken to separate these zones: characteristic focal mechanisms, seismic patterns, geomorphic imprints, coupling data, historical large ruptures (asperities) and gravimetry data available in several studies (refer to Alvarado et al. 2017).

It is important to mention that Alvarado et al. (2017) proposed an agreed regional seismo-tectonic zonation based on the integration of extensive research available for the Central American subduction. Therefore, only slight deviations from this model are seen in the model we used, in which e.g. outer rise seismicity has different rates than those of the interplate seismogenic zone (Álvarez-Gómez et al. 2012) that were not considered in previous regional seismic hazard studies (Benito et al. 2012), is treated separately. Thus, we estimate seismic rates of one of the most seismic active regions along the CAM, the inter-plate seismogenic zone, that has triggered most tsunamis in the region and separate the outer rise seismicity that could also generate tsunamis but with different rupture mechanism.

The tectonic segmentation of the Pacific side of Central America (CAM) is closely linked to the structures generated by the interaction of the Cocos, Caribbean, Nazca plates and the Panama block. The northern limit of the CAM is marked by the Motagua-Polochic fault system (PoF), a left-lateral shear zone that continues offshore along the Swan Islands transform fault. The PoF fault is a transform fault that accommodates deformation between the North American and the Caribbean plate. This deformation zone is a continuation of the Cayman tectonic system throughout the western Caribbean basin (Fig. S2). The transform plate boundary between the Caribbean and North American plates averages $18-20 \pm 3$ mm/yr of boundary motion (DeMets 2001). On the other side, along the southeastern end of the Cocos Plate the aseismic Cocos Ridge, with 20 km thick buoyant crust, could have been underthrusting for $\sim$ 1–5 Ma (Lonsdale and Klitgord 1978; de Boer et al. 1988, 1995; Sallarés et al. 2003). The convergence rate of the Cocos plate varies from 7.5 cm/year in northern CAM increasing the velocity to 9.3 cm/year towards southeast Costa Rica (DeMets 2001; DeMets et al. 2010).

The characterization of the CAM inter-plate seismogenic zone varies from fairly high coupling ($\sim$ 0.6) offshore Chiapas towards low-coupling ($\sim$ 0.25) offshore Guatemala and El Salvador (Franco et al. 2012), providing one of the criteria for defining seismo-tectonic zones. For example, GPS studies indicate very low coupling off the Nicaragua

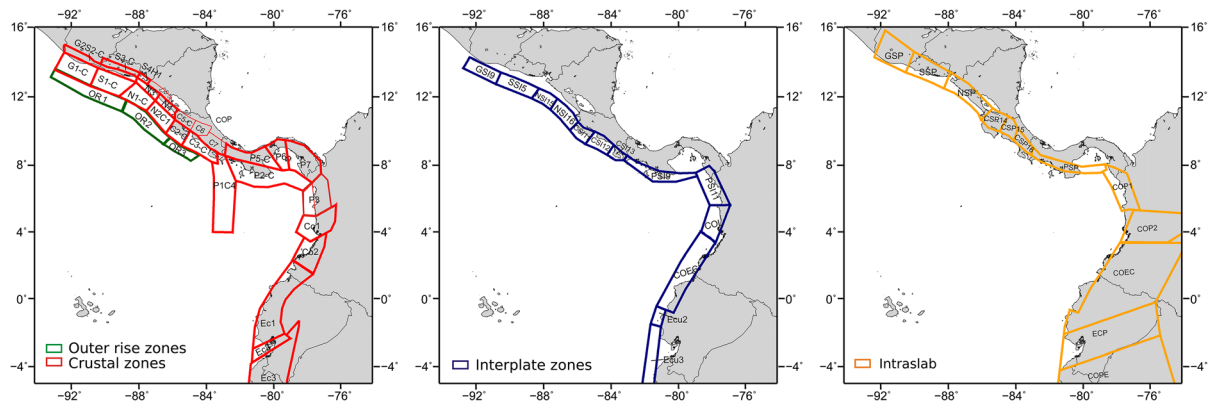

Figure 3
Delimitation of seismo-tectonic zones proposed for Central America, Colombia and Ecuador. The left panel shows outer rise zones (green) along the CAM together with the upper crustal zones along the Caribbean, the Panama block, the Andean block and the South American plate (red). Inter-plate zonation (subduction zone thrust earthquakes) is shown in blue at the central panel. The right panel presents zonation model for the intra-slab sources

and El Salvador segments (Alvarado et al. 2010; Correa-Mora et al. 2009; LaFemina et al. 2009). The low coupling has been explained by a lower interface normal stress due to the contact with the upper plate (Scholz and Small 1997; Protti et al. 1995). In contrast, the southern Central America margin has been proposed as a collision zone due to the Cocos Ridge subduction beneath the Panama block acting as an indenter (LaFemina et al. 2009). This feature could explain trench parallel velocities that dominate in Nicaragua (LaFemina et al. 2002). Based on the size of these segments, the maximum magnitude has been estimated from the scaling relations (Blaser et al. 2010). The latter scaling relations associate an area A to the magnitude moment Mw, and thus, one can estimate the seismic moment M_o. For that, we used the area of the segment following Aki's formula for the seismic moment (Aki 1966). The seismic moment (Eq. (1) of each segment of the megathrust is calculated based on its seismogenic area (A in km^2), mean slip δ and rigidity (μ) (here assumed as 30 GPa).

$$M_o = \mu A \delta, \tag{1}$$

The recurrence rates for the CAM-CE and the corresponding seismic parameters for each zone have been used as input data to the Monte-Carlo synthetic catalog generation technique. The seismic parameters for the inter-plate, crustal and intra-slab source zones are shown in Table 1. The seismic parameters such as b-value, earthquake annual rate and maximum magnitude have been estimated from the CAT2011 as explain in the next section. For the Colombian-Ecuador trench, seismic parameters within different zones were retrieved from the previous work by Beauval et al. (2013). A general geologic overview of the major seismic zones is given in the supplementary material.

2.2.1 Seismic Parameters

CAT2011 contains almost five hundred years of seismic records, but features a minimum magnitude Mw = 3.5 only after 1970. For the entire catalog, the magnitude of completeness (Mc) has been estimated as Mc = 4.0 after 1984 and Mc = 6.0 after 1821 according to the Stepp method (Stepp 1972). For each zone (Fig. 3), statistical seismic parameters lambda, beta, Mmin from the Gutenberg-Richter distribution (GRD) (Eq. 2) can be retrieved from the catalog by fitting the functional form of the frequency-magnitude distribution (FMD). In the present study, we employ the double truncated FMD as follows:

$$\lambda_{(Mi)} = e^{-\beta(M_i)} - e^{-\beta(M_{\max})} / e^{-\beta(M_{\min})} - e^{-\beta(M_{\max})} \tag{2}$$

where λ is the mean annual seismic rate, and $\beta = b \ln(10)$. The modified Gutenberg-Richter double truncated relation considers an upper magnitude bound, $M_{\max}$, since the rupture area of earthquakes

Table 1

Input data for Monte Carlo sampling for all seismo-tectonic zones considered in this study

Id	Depth (km)	Mw (min)	Mw (max)	Mw (max)	β	λ (4.5)	Rake	MFD
Outer rise seismic sources								
OR1	< 35	4.5	7.7	7.9	2.645	0.372	Normal	GR-T
OR2	< 35	4.5	7.7	7.9	2.64	1.431	Normal	GR-T
OR3	< 35	4.5	7.4	7.6	2.64	0.123	Normal	GR-T
Crustal seismic sources								
G1-C	< 15	4.5	7.5	7.7	2.42	1.115	Multi	GR-T
G2S2-C	< 20	4.5	6.7	6.9	2.107	0.28	Multi	GR-T
S1-C	< 25	4.5	5.8	6.1	3.694	0.601	Multi	GR-T
S3-C	< 15	4.5	6.8	7.1	2.105	0.974	Multi	GR-T
S4N5	< 20	4.5	7	7.3	1.95	0.992	Multi	GR-T
H1N4-C	< 20	4.5	6.3	6.5	2.429	0.315	Multi	GR-T
N1-C	< 15	4.5	7.8	8.1	2.96	3.584	Multi	GR-T
N3-C	< 25	4.5	6.8	7	2.033	0.291	Multi	GR-T
N4-C	< 25	4.5	6.5	6.7	3.172	0.178	Multi	GR-T
N2C1-C	< 15	4.5	7.3	7.5	3.006	4.524	Multi	GR-T
C2-C	< 15	4.5	7	7.1	2.091	0.352	Multi	GR-T
C3-C	< 15	4.5	7.5	7.7	2.309	1.098	Multi	GR-T
C4P1-C	< 30	4.5	7.7	7.9	2.615	16.206	Multi	GR-T
P2-C	< 20	4.5	7.3	7.5	1.992	2.267	Multi	GR-T
P3CO1	< 20	4.5	6.8	7	1.996	0.689	Multi	GR-T
P5-C	< 20	4.5	6.5	6.8	2.889	0.51	Multi	GR-T
P6-C	< 20	4.5	7.3	7.5	1.808	0.07	Multi	GR-T
P7-C	< 20	4.5	7.3	7.6	2.006	1.02	Multi	GR-T
CO2	< 20	4.5	7.1	7.3	2.07	0.11	Multi	GR-T
EC1	< 25	4.5	7.3	7.5	1.909	0.9	Multi	GR-T
EC2	< 25	4.5	7.5	7.7	2.208	0.34	Multi	GR-T
EC3	< 25	4.5	7.3	7.5	2.553	0.67	Multi	GR-T
Interplate source zones								
GSI9	8-40	4.5	7.9	8.1	2.383	5.32	Thrust	GR-T
SSI5	6-40	4.5	8.7	9	2.569	10.6	Thrust	GR-T
NSI15	6-40	4.5	7.9	8.1	2.834	8.99	Thrust	GR-T
NSI16	6-40	4.5	7.9	8.2	2.523	9	Thrust	GR-T
CSI11	6-40	4.5	8.1	8.3	1.914	2.24	Thrust	GR-T
CSI12	6-40	4.5	7.8	8.4	2.139	3.14	Thrust	GR-T
CSI13	6-40	4.5	7.6	7.8	1.9734	1.55	Thrust	GR-T
PSI9	20-40	4.5	7.7	7.9	2.086	1.155	Multi	GR-T
PSI11	20-100	4.5	7.1	7.3	1.971	1.008	Multi	GR-T
COL	5-40	4.5	7.9	8.1	2.3	3.02	Multi	GR-T
COEG	4-50	4.5	8.8	9	1.54	2.17	Thrust	GR-T
ECU2	4–50	4.5	7.2	7.5	2.346	0.86	Thrust	GR-T
ECU3	4–50	4.5	7.8	8	2.012	2.21	Thrust	GR-T
Intraplate sources								
GSP10	40–220	4.5	8.2	8.4	2.44	13.97	Multi	GR-T
SSP6	40–220	4.5	8	8.2	2.555	10.65	Multi	GR-T
NSP17	40–220	4.5	7.9	8	2.17	15.45	Multi	GR-T
CSP14	40–160	4.5	7.5	7.7	2.525	1.583	Multi	GR-T
CSP15	40–125	4.5	7.8	7.9	1.932	1.25	Multi	GR-T
CSP16	40–60	4.5	7.5	7.7	1.819	0.629	Multi	GR-T
PSP11	20–100	4.5	7.5	7.7	1.838	0.641	Multi	GR-T
COP1	> 100	4.5	7.5	7.7	1.02	0.502	Multi	GR-T
COP2	> 40	4.5	7.5	7.7	1.01	0.408	Multi	GR-T
COEC	50–150	4.5	7.5	7.7	2.78	2.17	Multi	GR-T
ECP	50–200	4.5	7.2	7.4	2.3	7.51	Multi	GR-T
COPE	50–150	4.5	7.5	7.7	1.9	3.53	Multi	GR-T
Interplate 1 zone CAM								
M9.0-1z	4–40	5.6	9.0	–	2.29	3.0	Thrust	GR-T

The only parameter varied within 2 models MCE and MEE was *Mmax* (truncation to Gutenberg-Richter relation). The upper bound *Mmax* for MEE model (left) and MCE (right). The λ is the annual rate of occurrence. Standard deviation for the depth sampling: 0.5. Multi refers to the variability of earthquake types assumed, this means a range of rakes used in each zone, are selected from the predominant rupture mechanism of past events. The rake range used for interplate zones varies between 75°–105°

and their slip are physically constrained. Further details of the estimation of maximum magnitudes are available in the supplementary material to this article. Earthquake occurrences (starting from the minimum magnitude) have been assumed to follow a Poisson process in time (Eq. 3). To be consistent with this premise, the seismic catalog has been de-clustered in order to avoid aftershocks in the seismic database, leaving only main or independent shocks.

$$P(H(x) > H_o, T) = 1 - e^{-\lambda(H(x) > H_o)(T)} \quad (3)$$

where P is the probability of exceeding a peak coastal amplitude (PCTA) threshold (H_o), λ is the mean annual rate of tsunami hits on a selected POI and T is the time window for the assessment.

In practice, seismic parameters for each zone were estimated from the regional earthquake catalogs using - Cosentino et al. (1977) and Kijko and Smit (2012). Based on the derived seismic zone parameters (Table 1), different synthetic seismic catalogs have been generated for each area of the fifty seismic zones ranging from Guatemala to Ecuador, and integrated into one single aggregated seismic catalog for the subsequent tsunami modeling. In fact, two comprehensive synthetic catalog were generated with the main difference in the upper bound ($M_{\max}$) of the GRD.

2.3. Synthetic Catalog Generation Procedure

To account for the randomness of the tsunami generation, the Monte-Carlo (MC) sampling for the fault parametrization was implemented to get the magnitude distribution as well as the multi-dimensional space of fault parameters and multiple sources of uncertainties (Rubinstein and Kroese 2008). The MC technique is an efficient tool to account for aleatory uncertainties by sampling different parameters (Ebel and Kafka 1999; Geist and Parsons 2006). The earthquake parameterization is thoroughly accounted for by assigning different ranges of focal mechanisms according to the characterization of the seismic sources.

In order to account for these uncertainties, we employed our code, *seisCat*. This code generates a synthetic catalog based on the frequency-magnitude distribution as well as distributions of other fault parameters (e.g., focal mechanism, geometry, depth distribution). Since source zones are determined in map-view (Fig. 3), the generation of a synthetic catalog additionally needs the distribution of earthquakes with depth within the given geographical limits. *seisCat* can be used as a means to distribute hypocenters uniformly inside a polygon with minimum and maximum depth levels (Sørensen et al. 2012), or project seismicity onto the predefined slab geometry uniformly or normally distributed.

Two reference synthetic catalogs have been developed, whose main difference lies in the upper truncation of the frequency-magnitude distribution. Whereas the first catalog corresponds to the expected earthquake (MEE) based on the expert opinion, the second catalog was compiled following the maximum credible earthquake (MCE) concept based on geological constraints. The maximum magnitudes in MCE appear to be larger particularly for some segments of the interplate seismogenic zones.

A third synthetic catalog has been included to test the effect of depth-dependent rigidity on hazard estimates. This catalog (MEE-r) is based on MEE and implements a rigidity profile as interpolated from estimations by Bilek and Lay (1999). Finally, a fourth synthetic catalog (M9.0-1z) considers the whole CAM megathrust as a single seismogenic zone capable to host up to M9 earthquakes (McCaffrey 2008). These two PTHA models will be presented in the Discussion section.

This synthetic seismicity has been generated based on the seismic parameters listed in Table 1. Sub-catalogs were developed employing the following criteria:

- Define the segment or polygon coordinates (Fig. 3) and the time window of 100 kyear to sample the synthetic seismicity. Within each segment we distribute epicenters randomly and uniformly
- The hypocenter of each earthquake is sampled from a uniform distribution. It is important to mention that this follows a three dimensional perspective (Fig. 4). In this study, the Slab1.0 slab geometry model (Hayes et al. 2012) is used to distribute seismicity within the different source zones by depth (Fig. 4). For instance, in case of inter-plate zones, earthquakes are distributed along the SLAB1.0 surface starting from 5–10 km depth toward to the down-dip limit, which follows the 40

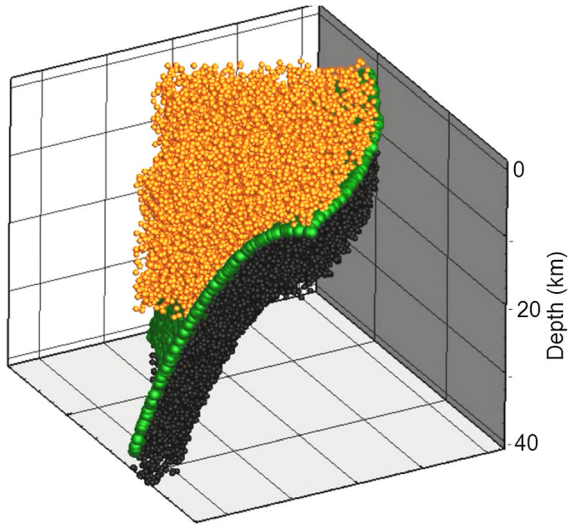

Figure 4
Synthetic earthquakes for the crustal, interplate and intraslab seismicity that has been sampled with Monte Carlo methods

km slab contour (50 km depth in Ecuador). For the upper crustal seismicity, scenarios are uniformly distributed from the surface down to 35 km depth. Similarly, the upper bound of the intra-slab synthetic events is provided by the Slab1.0 geometry.

- The magnitude (Mi) is sampled from the GRD's shown in Eq. (2). Figure 5 shows an example of the synthetic seismicity for all seismogenic zones.
- The fault size is obtained according to scaling relations to derive length (L) and width (W) for each sampled magnitude. These are estimated based on scaling relations for length and width in dependence of magnitude (Blaser et al. 2010). In addition, the latter provides a probability distribution function, which relates magnitude of the earthquake (Mi) to a corresponding width and length. This particular relation provides the variability given to the length that has important consequences in augmenting the variability of the rupture areas derived for each magnitude Mi.
- The slip is estimated with the seismic moment relation (Aki 1966; Hanks and Kanamori) as shown in Eq. (1).
- The strike for the inter-plate seismicity is sampled following the Slab1.0 model. For the cases of the upper crustal and intra-slab seismicity, we have applied a number of distribution intervals and gave weights for the distinctive ranges according to the prevailing azimuths of previous earthquakes in the GCMT catalog (Ekström et al. 2012), that are given at the bottom of Table 1.
- The dip angle variability follows a normal distribution based on the Slab1.0 model, or multi-ranges for the cases of upper crustal and intra-slab seismicity based on focal mechanisms of the GCMT catalog.
- The rake of each earthquake is sampled for different ranges using a multi-range choice, sampling from uniform and normal distributions (plus standard deviations) to increase variability. These ranges have been mostly used for upper crustal and intra-slab seismicity where earthquakes have larger variability of mechanisms. We have applied number of distribution intervals and gave weights for the different ranges according to the observed prevailing rake values of previous earthquakes. In the case of the outer rise, pure normal events were considered. Contrary, for the inter-plate seismogenic zones, a range of thrust events were assumed.

2.4. *Tsunami Modeling*

The set of multiple synthetic seismic catalogs allows for longer seismicity time span and a larger variability of fault parameters. These seismic catalogs corresponding to a window of time of 100 kyear are used to first simulate initial conditions for tsunami modeling. A threshold moment magnitude Mw = 6.4 is used. Each of these seismic events in the catalog has been simulated using the *easyWave* code that solves the linear long shallow water equations (LSWE) on a finite-difference staggered grid. *easyWave* employs Okada's (Okada 1985) dislocation model to calculate initial conditions for tsunami propagation from a set of fault parameters. The bathymetry used in this model is Gebco with one minute resolution (Becker et al. 2009).

easyWave employs fully reflecting boundary conditions along the coast. This means the code does not compute inundation and runup in an explicit way. Instead, we used indirect metric in order to assess the tsunami impact at the coast. We followed Kamigaichi

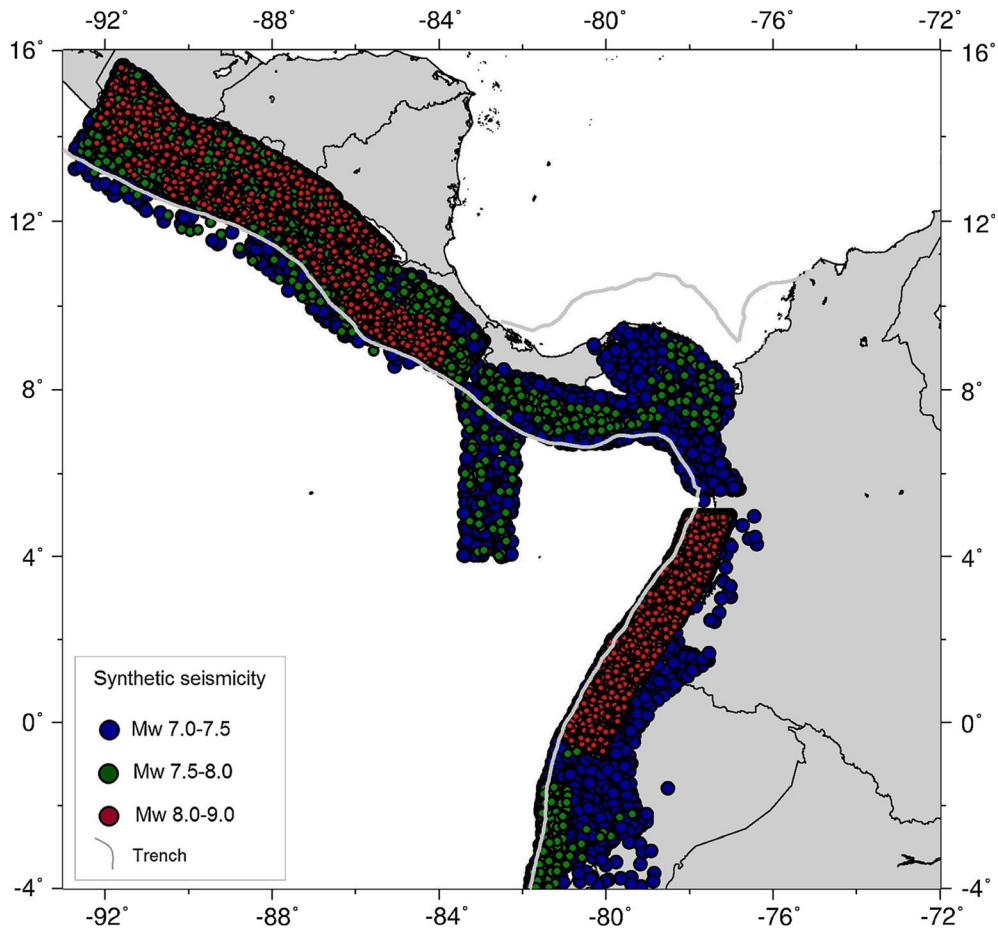

Figure 5
Map of the synthetic catalog used for model MEE containing about 184 k earthquakes Mw > 6.4

(2009) who suggested to record the wave height at some off-shore position, typically at 100 m depth, and then project this value to the coastline using the Green's Law (GL), as implemented for the Japanese Tsunami Early Warning System. In our computations, we saved maximum wave heights at water nodes located within 0–200 m depth interval. The post-processing procedure allowed us to select corresponding water nodes from the thousands of points along area of interest and to project their off-shore wave heights to the points of interest (POI) along the coast. This projection gave us our main metric: peak coastal tsunami amplitude (PCTA). Coastal tectonic correction (for the co-seismic uplift or subsidence) was additionally applied to the coastal POIs. Figure 6 shows the distribution of POIs used in this study, representing the selected coastal cities and harbors from Guatemala to southern Ecuador.

For this study, we have considered the Green's Law approach since nowadays precise modeling of the tsunami propagation and coastal impact over high-resolution nearshore bathymetry is still not feasible for regional-scale PTHA studies due to a lack of suitable high-resolution digital elevation models for the Pacific coast of Central America. Besides, even if high-resolution ($\sim$ 10–30 m) bathymetry models would be available, it is still computationally infeasible to model nearshore wave propagation for hundreds of thousands or millions of seismic scenarios needed for a full PTHA. There are examples of several local PTHA studies (e.g., González et al. (2009) for Seaside, Oregon; Lorito

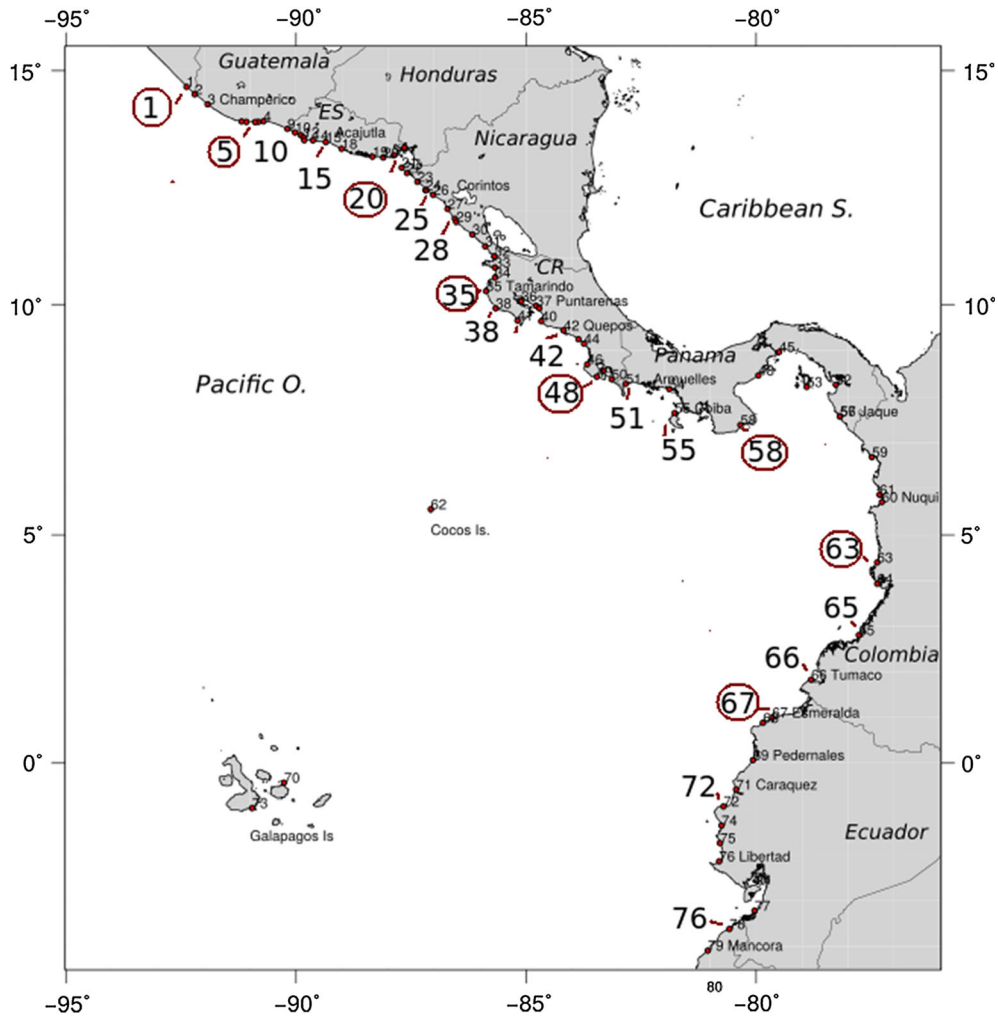

Figure 6
Map showing the location points of interest (POI) for the hazard estimates. Numbers refers to the POI number and selected coastal cities are shown as reference. *ES* El Salvador, *CR* Costa Rica

et al. (2015) for East Sicily), but the authors are not aware of any country- or regional- scale PTHA studies operating with high-resolution bathymetry models. Therefore, a first necessary step is to acquire reasonable amplification factors on the region as discussed by Hébert and Schindelé (2015). Due above reasons, regional-scale PTHA have to employ various approximations of the coastal impact from the coarse-resolution offshore propagation. Green's law is the most used and the most straightforward approximation accounting for the 1D wave shoaling. Because it has a singularity at zero water depth, wave height is usually projected to 1 m depth. Recently, several studies (Gailler et al. 2017; Glimsdal et al. 2019) proposed alternative methods of local amplification factors, which may better account for the particular nearshore bathymetry than the simple Green's law. The method suggested by Gailler et al. (2017), including the original scheme by Jamelot and Reymond (2015), requires either calibration to historical cases, or, again, simulations over very high-resolution bathymetry not available for Pacific Central America, and hence cannot be implemented in our study. The new method suggested by Glimsdal et al. (2019), in turn, does not necessarily require high-resolution bathymetry which makes it interesting for large-scale PTHA studies, on one side, but leaves open the question about its accuracy. In any case, the

method of local amplification factors should be considered as a valid alternative for future large- and regional-scale PTHA studies.

2.5. Hazard Estimates

The resulting PCTA's are aggregated to provide hazard curves and hazard maps where the average return times of i.e. 100, 500, 1000 and 5000 years can be retrieved for different wave heights. Probabilistic analysis provides a good method to evaluate the most important tsunamigenic sources that are contributing to hazard for any specific POI.

Thus, in the Discussion section we used probabilistic maps that also show the expected PCTA with annual exceedance probabilities for 0.02, 0.01, 0.002, 0.001, 0.0002, which corresponds to the inverse of 50, 100, 500, 1000, 5000 years return time, respectively. The alternative tsunami hazard models are derived from different assumptions within a sensitivity analysis approach. If high resolution bathymetry is available for the region, additional tsunami inundation modelling will account for nonlinear processes and effects of bottom friction, that are not accounted in this study. Therefore, probabilistic inundation maps are not provided.

3. Results

PTHA results are presented for the two different synthetic catalogs. These results are shown as hazard curves for selected sites as well as probability maps. To facilitate analysis, most of the results will be given for the MEE model. A comparison between the two models will be provided in the discussion section.

A hazard curve represents annual probabilities of exceedance of different tsunami wave heights (or herein PCTA) at specific locations. It integrates wave heights resulting from all the sources coupled with their probabilities. Calculated hazard curves for selected POIs are shown in Fig. 7. Refer to Fig. 6 for the POIs location. Overall, these hazard curves illustrate that significant tsunamis display very low annual probabilities of exceedance in the whole region.

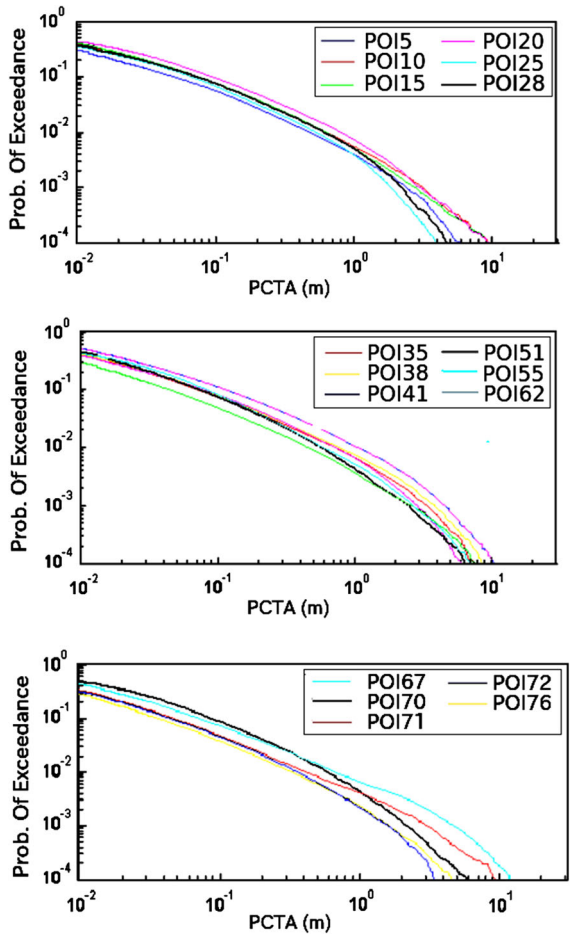

Figure 7
Upper, Hazard curves show the annual probability of exceeding a certain threshold for selected POIs from Guatemala to Nicaragua. Middle panel, hazard curves for selected POIs from south Nicaragua to Panama. Below, hazard curves for selected POIs from Colombia-Ecuador

The hazard curves for central and southern Central America have a distinct tail, which denotes a higher hazard with respect to the hazard in northern Central America (e.g. Guatemala). Notably, at shorter time windows of 50 year hazard appears very low with annual exceedance rates that are higher for southern Nicaragua, Costa Rica and Ecuador. Another observation from Fig. 7 is that overall in South America, annual probabilities of exceedance for larger PCTA's at 100 average return period (or i.e. the 1% probabilities on any given year) are higher than in Central America, except for southern Nicaragua, Costa Rica and specific coastal areas in Panama such as POI51 Armuelles and POI55 Coiba Island).

These tails in the hazard curves varies mainly in the coastal region of South America (Fig. 7). This can be related to the likelihood of larger events along the Colombia-Ecuador subduction zone or to the directivity of tsunami waves from sources of CAM that will not affect this particular sites, only in the long term where larger earthquakes are expected. This highlights the fact that very large tsunamis are expected with relatively larger return periods, which still not reconcile the 1992 and 2012 runups seen in a local scale (Fig. S3).

In summary, the examination of the hazard curves reveals that at the northern region of Central America tsunami probability is lower. This might be explained partially due to the wave directivity from southern seismic sources affecting mostly Nicaragua and Costa Rica.

An alternative way to show annual probabilities is presented on a map view showing the expected tsunami wave heights for specific mean return periods (times) or rates of exceedance. Here, the expected PCTA has been estimated for the 50, 100, 500, 1000, 5000 years.

In Fig. 8, we present the expected PCTA at selected locations for mean return periods according to the MEE model. The 50 years PCTA becomes higher towards the south, but generally does not exceed 1.0 m.

The largest PCTA for the 100 year mean return period are expected in Colombia-Ecuador (MEE model), while one of the maximum expected values corresponds to POI63. Furthermore, for the 1% annual exceedance probabilities, the expected PCTA lies within 1.5 m (MEE model). In this time frame, the most affected regions are still southern Nicaragua (POI26–POI30) and central-south Colombia (POI63–POI66). Along Panama, the highest hazard is posed by the South American seismic sources. Mainly along the coastal areas of Armuelles (POI51) and Chiriquí (POI54), expected PCTA of 1.5 m could be exceeded with a 1% annual probability. Similarly maximum tsunamis of about 1.5 m are expected in south Nicaragua.

In this case, with the current model, the 1% annual probability PCTA's values are not expected to overcome 2 m in the region as resulted in this model. The latter could highlight that larger recurrence rates are estimated from the frequency-magnitude distributions than might be expected, specially from the the Colombia-Ecuador interplate earthquakes where large earthquakes are known to have occurred in the last century.

These events, like the 1906 Colombia earthquake, appear to have long-term recurrence times. This means that in the longer return periods the hazard for Central America could be also dominated by large events expected from this subduction zone.

For the 500-year mean return period, tsunami hazard is higher in regions of South America characterized with PCTA values of 4 m (POI63). The estimated PCTA for the 500 year event is 3 m for both southern Nicaragua (POI25 to POI30) and Esmeralda, in Ecuador. Moreover, the tsunami hazard in Cocos island (Costa Rica) for the 500 year return period is about 2 m, and at the Galapagos Island PCTAs are expected to have about 2.5 m.

The PCTA for 1000 year event is estimated to reach 5 m in Esmeralda and surrounding coastal regions, 4.5 m in southern Nicaragua, and 4 m in the central and southern part of Costa Rica. Lowest hazard is expected in the regions of the Galapagos islands and Carate, southern Costa Rica as well as Cocos island, Here, PCTA is estimated to be 3 m.

In Central America, PCTAs are not expected to exceed 12 m. The hazard map shows that events corresponding to the 5000 year average return period have the highest hazard with 10 m as shown for reference in POI67 (Esmeralda). The run-up distribution from historical records showed in the last panel of Fig. 8 and Fig. S2 can provide an idea of the most affected coastal regions, and our results do not fully agree with that distribution. In the latter, the annual exceedance probability has been given for different return periods, showing only an agreement with larger tsunamis occurring along the southern Nicaragua coast and in Colombia-Ecuador. The coastal points (POI55 and POI58) are showing higher hazard. These coastal cities in Panama appear to be largely affected by tsunami directivity from the Colombia-Ecuador Trench, considering that the Panama seismic sources have smaller rates.

We further provide the hazard expressed as the probability that PCTA (assessed for a threshold of 2 m) will be exceeded at least once in a certain period

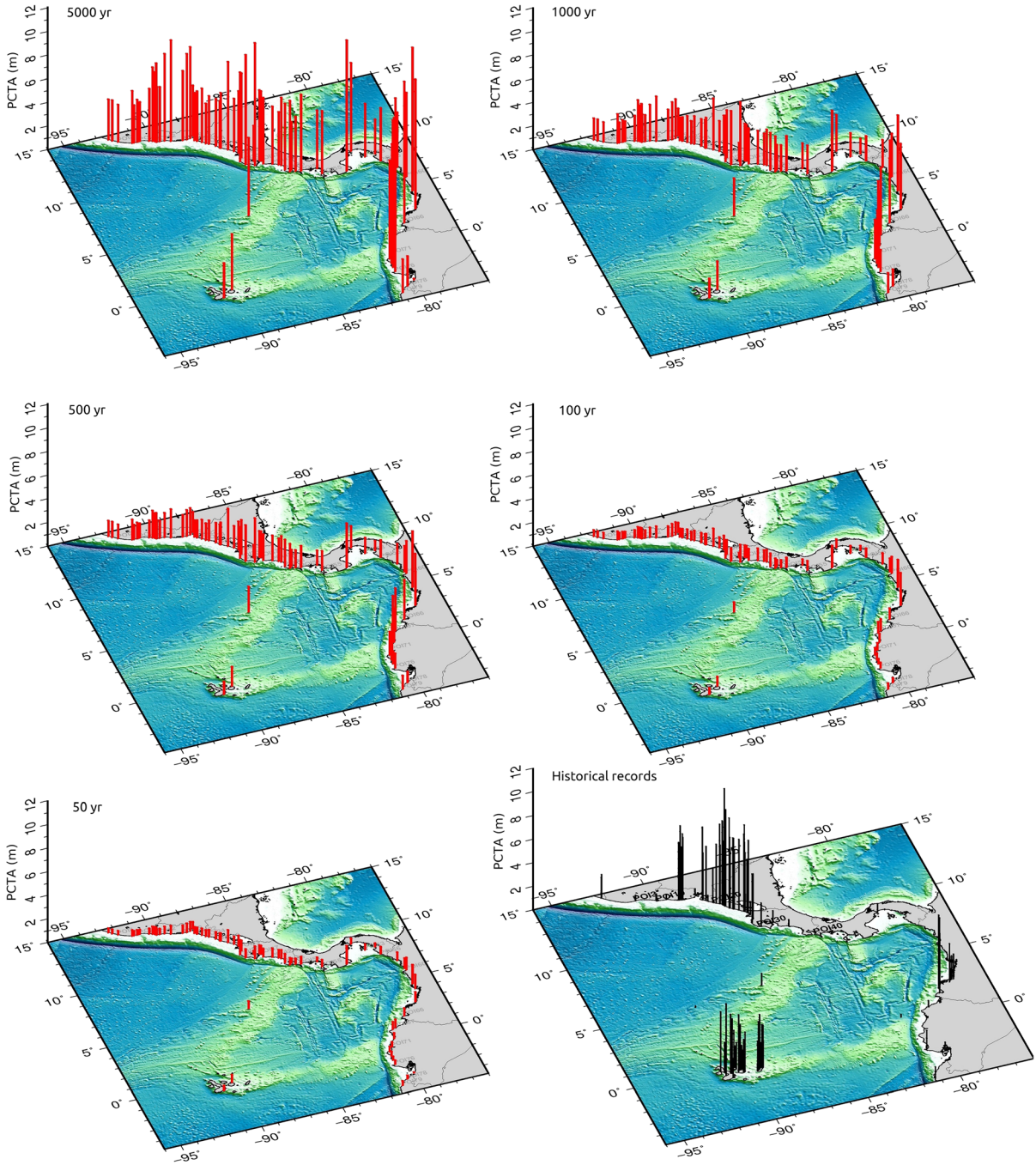

Figure 8
Hazard map showing the PCTA expected at mean return periods of 50, 100, 500, 1000 and 5000 years. The tsunami records shown in the last map (bars in black) are based on NGDC/WDS (2017). These results correspond to the MEE model

of time, as shown by the Eq. 3. In this case, the Fig. 9 shows probabilities of PCTA to reach specific values during the next 100 years.

Figure 10 shows aggregated wave heights exceeding certain thresholds for selected POIs. The hazard estimates have been grouped for northern

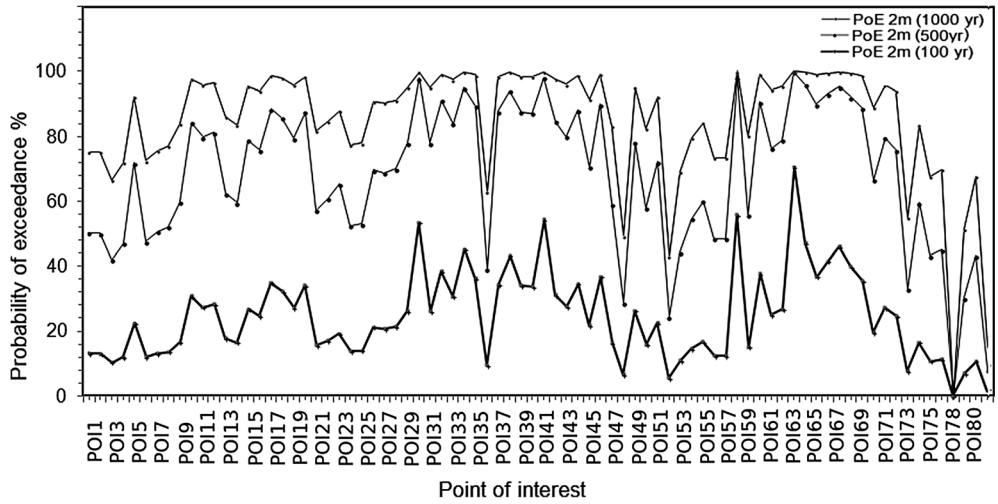

Figure 9
Probability of exceeding 2 m in for different times at selected POIs given in percentage. Refer to Fig. 6 for the POI location

CAM (upper panel), southern CAM (mid panel), and South America (lower panel). The tails of these curves varied significantly as seen in the plots of the upper panel. These curves correspond to three POIs in Nicaragua where maximum magnitude expected for the 100 year. The hazard in the POIs in Nicaragua decreases from north to south. Particularly, POI25 to POI29 show the higher hazard in these selected POIs (Fig. 10).

The hazard posed to Costa Rica is higher along the central Pacific coast POI42-POI44 (e.g. Quepos) than the POI48 (Carate) located about 140 km south of Quepos. The difference in the tail of the hazard curve for POI51 (Puerto Armuelles) could be related to a greater influence of several tsunamigenic sources from South America due to its location if compared to the other sites in Central America.

The results shown here are consistent with the fact that a variation of PCTA at different return periods is related to longer occurrence rates of large events mainly at the Ecuador-Colombia trench and Nicaragua. Also, we show in the following figure that large tsunamis could strike Central America with PCTA of more than 30 m (Fig. 11). Here, we show the maximum tsunamis extracted from the 100 kyear of simulations. However, as expected they appear to have very long recurrence times and are not well represented in the hazard curves. From Fig. 11, we can conclude that the influence of the maximum magnitudes, or upper bound that has been considered in the second model (MCE) leads to larger PCTAs in most of the POIs. We suggest that the local sources along northern Central America are increasing the hazard values, which are the ones whose upper bound was assumed larger.

Overall, these results show that local tsunamigenic sources have a higher influence in the hazard at e.g. the 500 year tsunami event, which is partially consistent with findings in other regions as suggested in other studies (González et al. 2009) but not necessarily in the regional sources. Also, variations in the hazard are reflected in the comparison of the two models with different maximum magnitudes (Fig. 12). The plot shows larger differences for the longer return periods comparing the two models based on the probability of exceeding a PCTA threshold of 2 m, where the maximum Mw is the only assumption that was changed to generate a second set of synthetic catalogs.

4. Discussion

4.1. Comparison of results with previous studies

The results for our two main models appear to differ with other regional studies. Figure 8 shows the PCTA expected for the mean return periods of

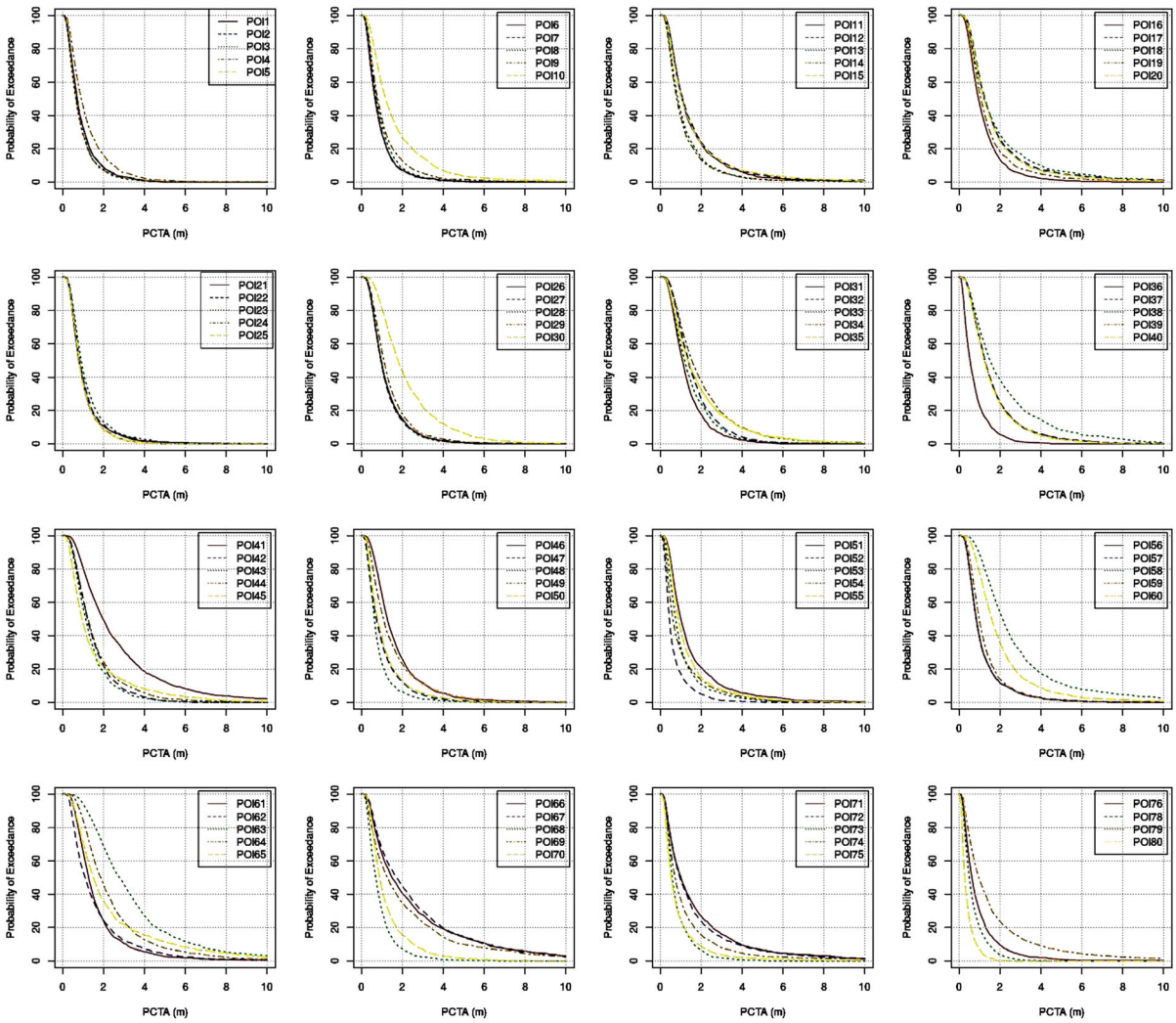

Figure 10
Probability of exceedance in 100 years in different POIS along CAM-CE. The probability is given as percentage. Refer to Fig. 6 for the POIs location

50–5000 years for the model MEE. The expected PCTA indicates rather low hazard level along most of the study area from Guatemala to Ecuador for the 50- and 100-year return periods. These results differ from those presented recently by Brizuela et al. (2014).

One reason for this difference could be the influence of b-values in the hazard curves. In their study, a seismic b-value of 0.67 is used to estimate earthquake recurrence rates for the entire region between south Mexico and Costa Rica (Brizuela et al. 2014), which not necessarily characterizes each zone. As shown by Hoechner et al. (2016), the b-value can have a large effect on the hazard estimates, therefore this could be one of the reasons of the highly different hazard estimates of these two studies.

Another explanation may be that since Brizuela et al. (2014) did not employ tsunami propagation simulations but instead used simplified source-to-coast tsunami run-up relations; our PTHA results differ from this due to the propagation component of the assessment chain. It would be very important to compare the two studies using the same input data in order to define where these differences arise and how to overcome them. Since results appear to be so

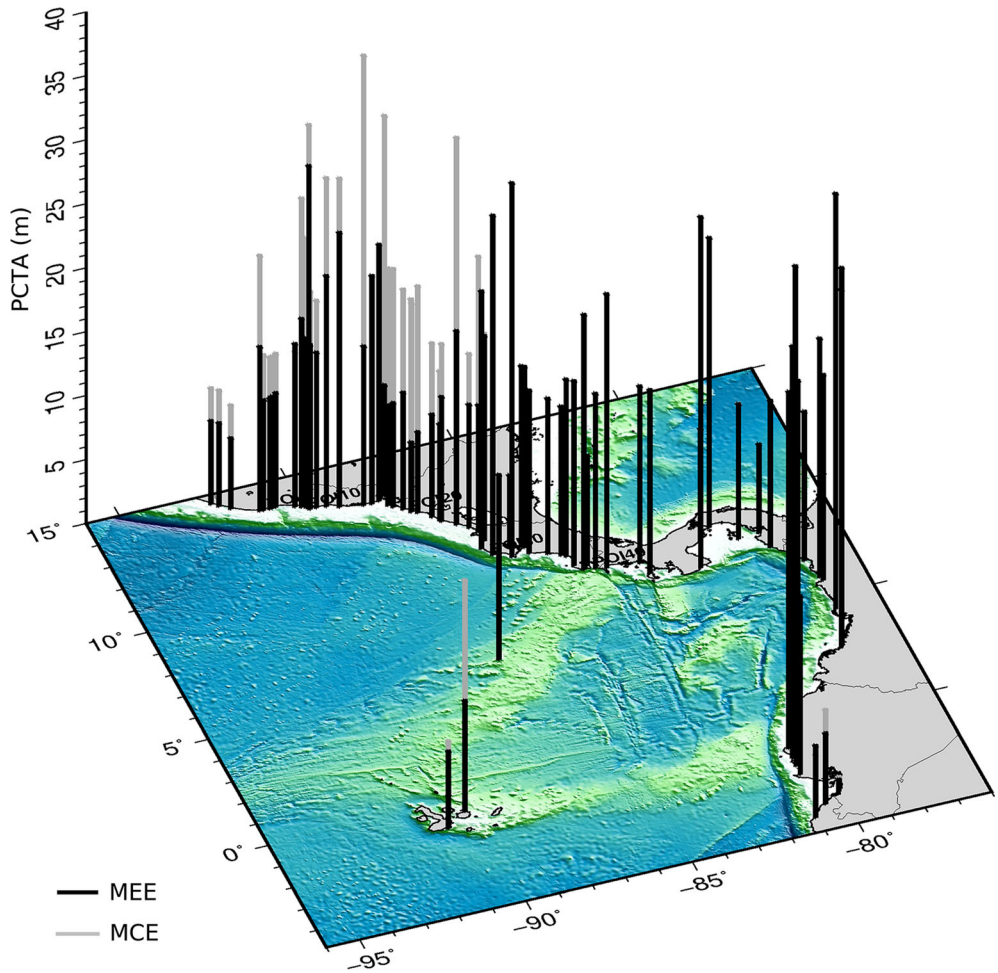

Figure 11
Maximum PCTA values extracted from all tsunami simulations. The black bars show the MEE model, and the MCE model is shown in gray. These large values in the map represents PCTA with larger return periods of those assessed in this study

different, it is necessary that future studies assess what causes these large discrepancies.

In this sense, Stein et al. (2017) have described that in principle the data and time windows used to describe the past seismicity of any region, as well as the models that are implemented to forecast future earthquakes will greatly effect the hazard estimates. The latter has been illustrated in regions with extensive paleotsunamis that have shown repeating large earthquakes and tsunamis (e.g. Cascadia, Chile), where a difference in seismic rates could be seen between assuming clustering of events different to the mean estimates (Stein et al. 2017). Thus, in this study we partially approach these uncertainties, and more models might be needed. Unfortunately, paleotsunami data showing longer recurrence rates that could be included in the hazard estimates is lacking in the CAM region.

Besides, Fig. 1 and Fig. S3 provide evidence of existing patterns of 500 years of tsunami data. The remarkable fact that the 1992 Nicaragua and the 2012 El Salvador tsunamis have been caused by moderate magnitude tsunami earthquakes, posing a hazard that could be inferred within the 1000 and 5000 year return periods. Both earthquakes generated larger tsunamis that could be expected from their moment magnitudes and hence could be characterized as 'tsunami earthquakes' (Kanamori 1972). Such

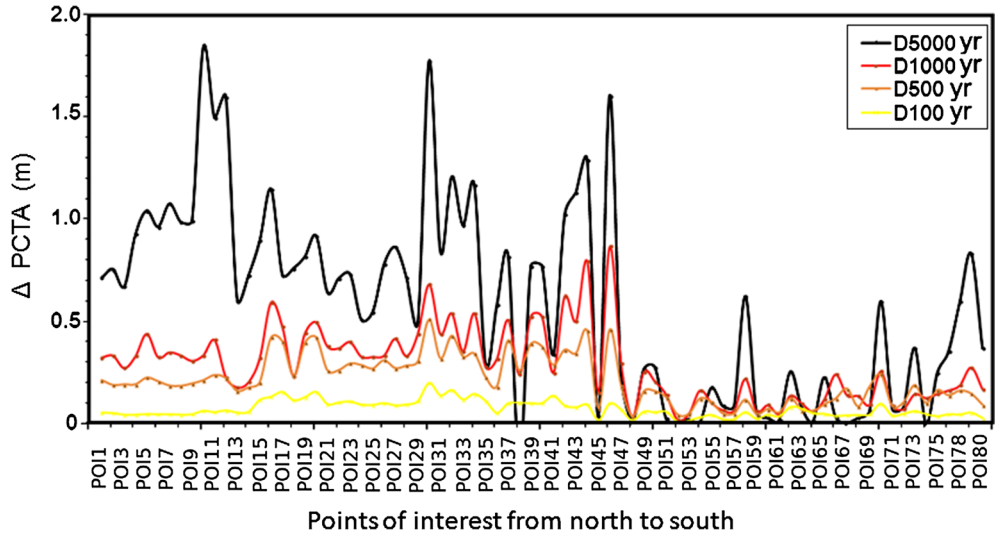

Figure 12
Difference in the PCTA between the two models (MCE and MEE) considered in this study to compare effect of Mmax. These differences are based on the threshold of exceeding 2 m wave height in the time (i.e. difference D5000 shown for the 5000 year time exposure is shown in gray)

earthquakes may release more co-seismic slip by rupturing weaker crustal material close to the trench (e.g., sediments). We consider lower rigidity estimates or concentration of shallow slip in our models. Thus, including more physical assumptions to the models and not only maximum magnitudes has highlighted the large dependency that PTHA has on the fundamental assumptions. Further studies comparing different methods will shed light on this aspect that is crucial for the tsunami hazard assessment because this dependency on the choice of the probability models (Stein et al. 2017).

4.2. *Sensitivity analysis*

To further understand the susceptibility of hazard estimates to major model assumptions, we considered two additional synthetic catalogs (ref. to Sect. 2.3 above). One of them (MEE-r) is based on our MEE reference catalog but implies depth-dependent rigidity in accord with Bilek and Lay (1999). This rigidity model (applied only to the CAM inter-plate seismogenic zone) accounts for the phenomenon of 'tsunami earthquakes'. Since in the present approach we model ruptures with the classical single 'Okada' fault model, we had to assume an effective rigidity value for the whole fault plane (e.g., no rigidity variation along the rupture width). This effective rigidity value was, in turn, picked from the depth-dependent rigidity profile according to the depth of the center of the fault. For ruptures with large width, this approach may result in the overestimation of their tsunamigenic potential, therefore we may consider this model as a 'rigidity end-member' model in our sensitivity analysis. Figure 13 compares PTHA results between the constant and depth-dependent rigidity models.

In this sense, there is relative agreement with the section of Nicaragua to Costa Rica in terms of the size of tsunami, showing that local segments prone to tsunami earthquakes could greatly contribute to the tsunami hazard posed in Central America and appear to be underestimated in our reference models MEE and MCE.

Thus, the distribution of run-ups clustered in three segments in all models through the area of this study, that corresponds with few events (Fig. 1 and S3). In Nicaragua, for example, most of the run-up values are related to the 1992 earthquake, and in Colombia-Ecuador, most of run-ups were generated from the 1906 and 1979 Colombia-Ecuador earthquakes. What seems to be consistent in the shorter term is that tsunami hazard is higher in Nicaragua and southern

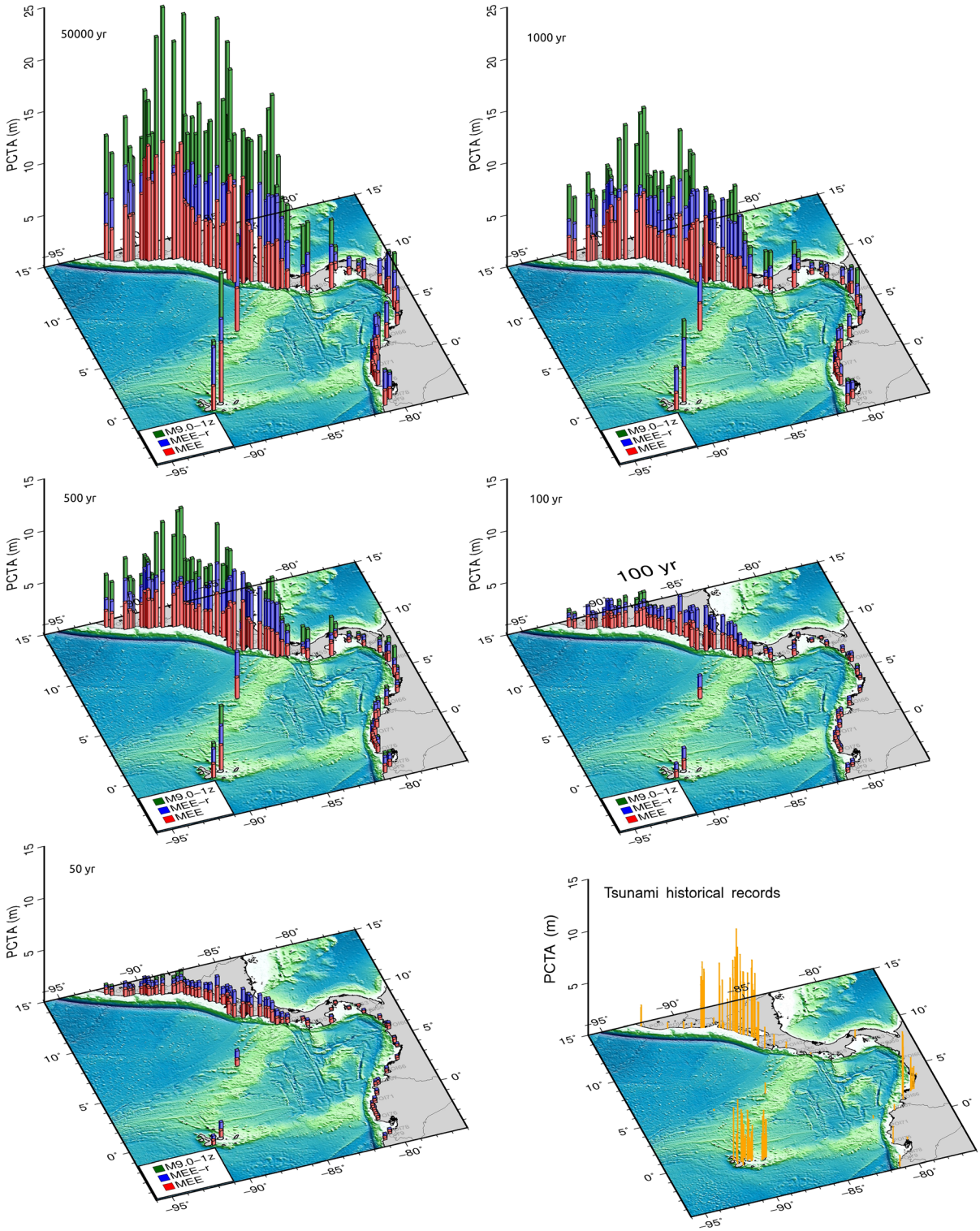

Figure 13

Each map shows the PCTA expected for several return periods for three models based only on the CAM interplate seismogenic zone. MEE stands for the same model shown in Fig. 8. MEE-r model includes the rigidity depth variation. M9.0-1z stands for the CAM single segment with uniform rigidity similar as it was used for MEE and MCE models. Refer to Table 1 to see the seismic parameters

Colombia to Ecuador. Particularly for Central America, the hazard curves show higher hazard in southern Nicaragua and Costa Rica in the long term (e.g POI31, POI35, POI41).

Additionally, we explore another source of uncertainty which is related to the seismo-tectonic segmentation and is associated to the earlier idea of McCaffrey (2008) that we cannot rule out that any subduction zone may produce a magnitude 9 or larger earthquake. Following this idea, we show hazard estimates by assuming the whole CAM megathrust as one single segment with Mmax 9.0 (model called 'M9.0-1z'), as shown in Fig. 13. As might be expected, significantly higher PCTA refer to the *large return periods* (> 500 years) due to the long recurrence rates of giant earthquakes. In the shorter perspective (return periods of 50 and 100 years), the effect of low shallow rigidity (i.e., 'tsunami earthquakes') becomes dominant. Also, it is observed from the hazard curves that the MAT poses a low tsunami hazard to coastal towns in South America.

4.3. Limitations of the Models

The limitations of the carried out model are related to the large spectrum of uncertainties which have been only partly accounted. Some of the assumptions such as Poisson process could be treated as epistemic uncertainty when alternative models such as Brownian Passage Time process (Matthews et al. 2002) are considered. This could hold e.g. for the short term forecasting that accounts for the fault interaction or aftershocks. However, for the mid-to-long-term assessment, the Poisson process is realistic and valid in PSHA as well as PTHA (Horspool et al. 2014; Parsons and Geist 2009b). Yet, a remaining point is the need to integrate more assumptions and spatio-temporal statistic techniques, that could constrain if the earthquake rates are solely controlling what appears to be low hazard estimates.

A physical limitation in PTHA derives from the simple rupture scenarios based on uniform slip, neglecting critical aspects such as the slip distribution influence on tsunami inundation (Li et al. 2016). In the case of the slab model, slip should be distributed within sub-fault models, but we didn't perform this in a stochastic way. Randomness is in turn given by the stochastic location of earthquake sources and the focal mechanisms, which have a high influence in local tsunami PCTA. More physical constraints have to be considered in PTHA models (Murphy et al. 2016). For example, in most of the models discussed here, we assumed uniform slip and a constant shear modulus of 30 GPa. Alternatively, we considered variations of the shear modulus along-dip. Allowing depth-varying shear modulus greatly influenced the hazard estimates. Such assumptions could provide different branches in the construction of a logic tree to integrate more uncertainties.

We identify three major limitations of our model. First, while we compared models for two maximum magnitudes truncating the GRD based on a regional model (Alvarado et al. 2017), we did not account for many alternative segmentation models that allow different maximum magnitudes nor the zone-less approach except for one case where the CAM is assumed to rupture free of segments with the possibility of earthquakes up to Mw 9.0. This could be critical since large earthquakes could rupture beyond the proposed segment limits (Okal et al. 2006) as shown in our model when considering mega-earthquakes in the one-segment interplate seismogenic zone that lead to larger PCTA in long return periods. Second, we restrict the assessment only to earthquake sources. An aspect that should be included in future work is to account for the tsunami hazard due to submarine landslides. Particularly, in Central America, significant slide imprints resembling large submarine landslides have been imaged (VonHuene et al. 2004), but their probability of occurrence is difficult to constrain. Third, we did not consider trans-Pacific events that are known to affect Central America (Rabinovich et al. 2013; Chacón-Barrantes and Gutiérrez-Echeverría 2017). In Fig. S3, we separated the recorded runups in the study area to highlight that the Galapagos and Cocos islands are exposed to long distance tsunamis as has been recorded by the 2011 Tohoku earthquake (yellow bars). Including this multi-hazard approach will give a more complete probabilistic assessment for this region. Another aspect that could affect the hazard variations in short distances are the bathymetric features in Central America. These differ in very clear segments, since the basin offshore Central

America is prone to edge waves. Those particular types of waves occur due to refraction and travel parallel to the coast. They can be typical of the shallow continental shelf as seen from numerical simulations (Zamora and Babeyko 2015).

4.4. Validity and Reliability of the PTHA

The main approach proposed for probabilistic seismic hazard assessment testing is addressed by comparing the overall forecast with ground motion data (Stirling and Gerstenberger 2010). Similar to that approach, the PTHA has to be tested. Nonetheless, the historical observations of wave heights along the coast of Central America, as in many other regions in the world is too short in duration, which disables the ability to make a robust testing. In this study, a qualitative comparison has been done by comparing wave height distribution given by tsunami catalog and the results for 500 and 1000 year return period. It has to be kept in mind that some tsunami records are given as run-up values and others as wave height (Fig. 1b).

Finally, the ultimate goal of the PTHA is to provide a forecast for the frequency of future tsunamis at selected coastal regions. This approach uses statistical analysis, which should be tested rigorously. However, unlike in probabilistic seismic hazard assessment (PSHA), where a set of algorithms have been implemented to test seismic hazard assessment (van Stiphout et al. 2011) based on short term observations, such testing is not realistic for tsunami hazard. However, future work should be planned to test for more tsunami hazard assessment techniques in this region, where 500 years of data might not be sufficient since the coastal areas were not always populated, thus the tsunami records could be incomplete to compare with the mean recurrence times of tsunamis in this region.

5. Conclusions

This study has embraced a comprehensive probabilistic tsunami approach to estimate hazard at specific POIs from Guatemala to Ecuador. Our approach is based on combining the assessment of seismic sources with numerical simulations of tsunamis. This method has the advantage of providing tsunami frequency based on exhaustive seismic data along Central America.

After establishing the seismic zonation based on a total of 50 individual seismic area sources, the Monte-Carlo approach was used to simulate a series of synthetic regional earthquake catalogs for the next 100 kyear. Monte-Carlo sampling from the multi-dimensional fault parameter space allows random uncertainties in the rupture process to be taken into account. In addition, the numerical simulation of tsunami wave propagation also considers bathymetric imprints that could affect the waveforms and additionally explain the variability of PCTA. The time span is something that has to be tested, for such studies larger time span (e.g. 500 kyear–1 myear) could be advisable to cover more seismic cycles, especially for the segments with longer recurrence times.

This numerical approach has an advantage over other studies, as it combines a great variability of parameters with realistic tsunami propagation, yet is too computationally expensive. Therefore, in a following paper, Tsunami Green Functions are used to facilitate this assessment and the sensitivity analysis. Two synthetic seismic catalogs resulted from joining fifty seismic zones, from Guatemala to Ecuador. Each catalog contains about 185,000 earthquakes larger than Mw 6.4. The two catalogs differ in the assumptions on their maximum magnitude. For each earthquake tsunami generation and propagation for 6 h were simulated and maximum wave heights saved at the thousands of near-coastal computational nodes, located within the depth interval from 0 to 500 m. In the post-processing phase, these wave heights were projected onto the selected 80 coastal POI's by means of the Green's law. To facilitate the analysis, hazard curves were presented for fewer POIs.

Our analysis shows that tsunami hazard is higher in Nicaragua and Colombia, where the probability of exceeding 2 m in 500 years is 50–70%, respectively. For 50 and 100 years return periods, expected tsunami wave heights are rather small in the whole study area, and hazard appears to be low. In general, wave heights up to 1 m are expected for the 100 years return periods. The latter could be expected from the

historical tsunami catalogs, except for the 1992 and 2012 tsunami earthquake events that dominate the runup distributions along Central America if compared with all events occurred during the last 500 years.

The assessment with different assumptions such as different zonation for the interplate seismogenic zone and lower rigidity values shows a high variability of hazard estimates that cannot be neglected. The latter raise the question of the validity of results where only a reduced range of uncertainties are incorporated.

It is shown in this study that even when large magnitudes for Central America have been estimated for some segments, the hazard becomes significant only for higher return periods, which appears to be consistent with what has been argued from seismological and geodetic studies.

Ideally, after the various limitations described here have been addressed, this type of model that can cover various mean return periods could provide a foundation for engineers to modify tsunami building codes. In addition, evacuation and coastal planning have to be further developed in order to take into account future models of this type that cover different return periods, rather than simply basing them on maximum credible earthquake estimates.

Acknowledgements

This study was possible thanks to the financial support to NZ from the Helmholtz Association and the GeoSim Program and the GeoForschungsZentrum (GFZ-Potsdam). Deep thanks to B. Benito, Y. Torres, A. Rivas and R. García at the Politechnic of Madrid (UPM) for hosting NZ during the Central American PSHA Workshop held in 2011 and for the discussions on the probabilistic framework. Special acknowledge to W. Rojas, E. Molina, E. Camacho for discussions related to Central American seismic catalog and seismic rates of the region. M. Fernández is acknowledged for discussions of the Central America tsunami catalog. A. Hoechner is acknowledged for the fruitful discussions about PTHA uncertainties. M.Sørensen and L. Matias are acknowledged for comments on a first stage of the study. Most figures were drawn using the GMT software Wessel et al. (2013) and R-project (R Core Team 2014). We strongly appreciate the comments and suggestions of two anonymous reviewers and the guest editor of the special volume E. Okal.

References

Aki, K. (1966). Generation and propagation of G waves from the Niigata earthquake of June 16, 1964. *Bulletin of the Earthquake Research Institute*, *44*, 73–88.

Alvarado, D., DeMets, C., Tikoff, B., Hernandez, D., Wawrzyniec, T., Pullinger, C., et al. (2010). Forearc motion and deformation between El Salvador and Nicaragua: GPS, seismic, structural, and paleomagnetic observations. *Lithosphere*, *3*(1), 3–21.

Alvarado, G. E., Benito, B., Staller, A., Climent, Á., Camacho, E., Rojas, W., et al. (2017). The new Central American seismic hazard zonation: Mutual consensus based on up to day seismotectonic framework. *Tectonophysics*, *721*, 462–476.

Álvarez-Gómez, J. A., Meijer, P. T., Martínez-Díaz, J. J., & Capote, R. (2008). Constraints from finite element modeling on the active tectonics of northern Central America and the Middle America Trench. *Tectonics*, *27*(1), TC1008.

Álvarez-Gómez, J. A., Gutiérrez-Gutiérrez, O. Q., Aniel-Quiroga, I., & Gonzlez, M. (2012). Tsunamigenic potential of outer-rise normal faults at the Middle America trench in Central America. *Tectonophysics*, *574–575*, 133–143.

Álvarez-Gómez, J. A., Aniel-Quiroga, I., Gutiérrez-Gutiérrez, O. Q., Larreynaga, J., González, M., Castro, M., et al. (2013). Tsunami hazard assessment in El Salvador, Central America, from seismic sources through flooding numerical models. *Natural Hazards and Earth System Sciences*, *13*(11), 2927–2939.

Basili, R., Tiberti, M. M., Kastelic, V., Romano, F., Piatanesi, A., Selva, J., et al. (2013). Integrating geologic fault data into tsunami hazard studies. *Natural Hazards and Earth System Sciences*, *13*(4), 1025–1050.

Beauval, C., Yepes, H., Palacios, P., Segovia, M., Alvarado, A., Font, Y., et al. (2013). An earthquake catalog for seismic hazard assessment in Ecuador. *Bulletin of the Seismological Society of America*, *103*(2A), 773–786.

Becker, J., Sandwell, D., Smith, W., Braud, J., Binder, B., Depner, J., et al. (2009). Global bathymetry and elevation data at 30 Arc Seconds Resolution: SRTM plus. *Marine Geodesy*, *32*(4), 355–371.

Benito, M. B., Lindholm, C., Camacho, E., Climent, A., Marroquin, G., Molina, E., et al. (2012). A new evaluation of seismic hazard for the Central America region. *Bulletin of the Seismological Society of America*, *102*(2), 504–523.

Bilek, S. L., & Lay, T. (1999). Rigidity variations with depth along interplate megathrust faults in subduction zones. *Nature*, *400*, 443–446.

Blaser, L., Kruger, F., Ohrnberger, M., & Scherbaum, F. (2010). Scaling relations of earthquake source parameter estimates with special focus on subduction environment. *Bulletin of the Seismological Society of America*, *100*(6), 2914–2926.

Borrero, J. C., Kalligeris, N., Lynett, P. J., Fritz, H. M., Newman, A. V., & Convers, J. A. (2014). Observations and modeling of the August 27, 2012 earthquake and tsunami affecting El Salvador and Nicaragua. *Pure and Applied Geophysics*, *171*(12), 3421–3435.

Brizuela, B., Armigliato, A., & Tinti, S. (2014). Assessment of tsunami hazards for the Central American Pacific coast from southern Mexico to northern Peru. *Natural Hazards and Earth System Science*, *14*(7), 1889–1903.

Burroughs, S. M., & Tebbens, S. F. (2005). Power-law scaling and probabilistic forecasting of tsunami runup heights. *Pure and Applied Geophysics*, *162*(2), 331–342.

Chacón-Barrantes, S., & Gutiérrez-Echeverría, A. (2017). Tsunamis recorded in tide gauges at Costa Rica Pacific coast and their numerical modeling. *Natural Hazards*, *89*(1), 295–311.

Cornell, C. A. (1968). Engineering seismic risk analysis. *Bulletin of the Seismological Society of America*, *58*(5), 1583–1606.

Correa-Mora, F., DeMets, C., Alvarado, D., Turner, H. L., Mattioli, G., Hernandez, D., et al. (2009). GPS-derived coupling estimates for the Central America subduction zone and volcanic arc faults: El Salvador. *Honduras and Nicaragua, Geophysical Journal International*, *179*, 1279–1291.

Cosentino, P., Ficarra, V., & Luzio, D. (1977). Truncated exponential frequency-magnitude relationship in earthquake statistics. *Bulletin of the Seismological Society of America*, *67*(6), 1615–1623.

de Boer, J. Z., Defant, M. J., Stewart, R. H., Restrepo, J. F., Clark, L. F., & Ramirez, A. H. (1988). Quaternary calc-alkaline volcanism in western Panama: Regional variation and implication for the plate tectonic framework. *Journal of South American Earth Sciences*, *1*(3), 275–293.

de Boer, J. Z., Drummond, M. S., Bordelon, M. J., Defant, M. J., Bellon, H., & Maury, R. C. (1995). Cenozoic magmatic phases of the Costa Rican island arc (Cordillera de Talamanca). *Geological Society of America Special Papers*, *295*, 35–56.

DeMets, C. (2001). A new estimate for present-day Cocos-Caribbean plate motion: Implications for slip along the Central American volcanic arc. *Geophysical Journal International*, *28*(21), 4043–4046.

DeMets, C., Gordon, R. G., & Argus, D. F. (2010). Geologically current plate motions. *Geophysical Journal International*, *181*(1), 1–80.

Ebel, J., & Kafka, A. (1999). A Monte Carlo Approach to Seismic Hazard Analysis. *Bulletin of the Seismological Society of America*, *89*(4), 854–866.

Ekström, G., Nettles, M., & Dziewoński, A. (2012). The global CMT project 2004–2010: Centroid-moment tensors for 13,017 earthquakes. *Physics of the Earth and Planetary Interiors*, *200*, 1–9.

Fernández, M., Ortiz-Figueroa, M., & Mora, R. (2004). Tsunami hazards in El Salvador. *Geological Society of America Special Paper*, *375*, 435–444.

Franco, A., Lasserre, C., Lyon-Caen, H., Kostoglodov, V., Molina, E., Guzman-Speziale, M., et al. (2012). Fault kinematics in northern Central America and coupling along the subduction interface of the Cocos Plate, from GPS data in Chiapas (Mexico), Guatemala and El Salvador. *Geophysical Journal International*, *189*(3), 1223–1236.

Gailler, A., Hbert, H., Schindel, F., & Reymond, D. (2017). Coastal amplification laws for the French Tsunami warning center: Numerical modeling and fast estimate of tsunami wave heights along the French Riviera. *Pure and Applied Geophysics*, *175*, 1–16.

Geist, E. L. (2009). Phenomenology of tsunamis: Statistical properties from generation to runup. *Advances in Geophysics*, *51*, 107–169.

Geist, E. L., & Parsons, T. (2006). Probabilistic analysis of tsunami hazards. *Natural Hazards*, *37*(3), 277–314.

Glimsdal, S., Løvholt, F., Harbitz, C. B., Romano, F., Lorito, S., Orefice, S., et al. (2019). A new approximate method for quantifying tsunami maximum inundation height probability. *Pure and Applied Geophysics*, *176*, 3227–3246.

González, F. I., Geist, E. L., Jaffe, B., Kânolu, U., Mofjeld, H., Synolakis, C. E., et al. (2009). Probabilistic tsunami hazard assessment at Seaside, Oregon, for near- and far-field seismic sources. *Journal of Geophysical Research*, *114*(C11), C11023.

Grezio, A., Babeyko, A., Baptista, M. A., Behrens, J., Costa, A., Davies, G., et al. (2017). Probabilistic tsunami hazard analysis: Multiple sources and global applications. *Reviews of Geophysics*, *55*(4), 1158–1198.

Hayes, G. P., Wald, D. J., & Johnson, R. L. (2012). Slab1. 0: A three-dimensional model of global subduction zone geometries. *Journal of Geophysical Research: Solid Earth*, *117*(B1), B01302.

Hébert, H., & Schindelé, F. (2015). Tsunami impact computed from offshore modeling and coastal amplification laws: Insights from the 2004 Indian Ocean tsunami. *Pure and Applied Geophysics*, *172*(12), 3385.

Hoechner, A., Babeyko, A., & Zamora, N. (2016). Probabilistic tsunami hazard assessment for the Makran region with focus on maximum magnitude assumption. *Natural Hazards and Earth System Science*, *16*, 1339–1350.

Horspool, N., Pranantyo, I., Griffin, J., Latief, H., Natawidjaja, D. H., Kongko, W., et al. (2014). A probabilistic tsunami hazard assessment for Indonesia. *Natural Hazards and Earth System Sciences*, *14*(11), 3105–3122.

Jamelot, A., & Reymond, D. (2015). New tsunami forecast tools for the French polynesia tsunami warning system. *Pure and Applied Geophysics*, *172*, 791–804.

Kamigaichi, O. (2009). Tsunami forecasting and warning. In R. A. Meyers (Ed.), *Encyclopedia of Complexity and Systems Science SE-568* (pp. 9592–9618). New York: Springer.

Kanamori, H. (1972). Mechanism of tsunami earthquakes. *Physics of the Earth and Planetary Interiors*, *6*(5), 346–359.

Kijko, A., & Smit, A. (2012). Extension of the Aki-Utsu b-value estimator for incomplete catalogs. *Bulletin of the Seismological Society of America*, *102*(3), 1283–1287.

Knopoff, L., Kagan, Y. Y., & Knopoff, R. (1982). b Values for foreshocks and aftershocks in real and simulated earthquake sequences. *Bulletin of the Seismological Society of America*, *72*(5), 1663–1676.

Kobayashi, D., LaFemina, P., Geirsson, H., Chichaco, E., Abrego, A. A., Mora, H., et al. (2014). Kinematics of the western Caribbean: Collision of the Cocos Ridge and upper plate deformation. *Geochemistry, Geophysics, Geosystems*, *15*, 1671–1683.

LaFemina, P. C., Dixon, T. H., & Strauch, W. (2002). Bookshelf faulting in Nicaragua. *Geology*, *30*(8), 751–754.

LaFemina, P., Dixon, T. H., Govers, R., Norabuena, E., Turner, H., Saballos, A., et al. (2009). Fore-arc motion and Cocos Ridge collision in Central America. *Geochemistry, Geophysics, Geosystems*, *10*(5), 1–21.

Li, L., Switzer, A. D., Chan, C.-H., Wang, Y., Weiss, R., & Qiu, Q. (2016). How heterogeneous coseismic slip affects regional probabilistic tsunami hazard assessment: A case study in the South China Sea. *Journal of Geophysical Research: Solid Earth*, *121*, 6250–6272.

Lindholm, C., Redondo, C. A., & Bungum, H. (2004). Two earthquake databases for Central America. *Geological Society of America Special Papers*, *375*, 357–362.

Lonsdale, P., & Klitgord, J. (1978). Structure and tectonic history of the eastern Panama Basin. *Geological Society of America Bulletin*, *89*(7), 981–999.

Lorito, S., Tiberti, M. M., Basili, R., Piatanesi, A., & Valensise, G. (2008). Earthquake-generated tsunamis in the Mediterranean Sea: Scenarios of potential threats to Southern Italy. *Journal of Geophysical Research: Solid Earth*, *113*(B1), B1301.

Lorito, S., Selva, J., Basili, R., Romano, F., Tiberti, M. M., & Piatanesi, A. (2015). Probabilistic hazard for seismically induced tsunamis: Accuracy and feasibility of inundation maps. *Geophysical Journal International*, *200*(1), 574–588.

Løvholt, F., Glimsdal, S., Harbitz, C. B., Zamora, N., Nadim, F., Peduzzi, P., et al. (2012). Tsunami hazard and exposure on the global scale. *Earth-Science Reviews*, *110*, 58–73.

Løvholt, F., Khn, D., Bungum, H., Harbitz, C. B., & Glimsdal, S. (2012). Historical tsunamis and present tsunami hazard in eastern Indonesia and the southern Philippines. *Journal of Geophysical Research: Solid Earth*, *117*(B9), B09310.

Lyon-Caen, H., Barrier, E., Lasserre, C., a. Franco, I., Arzu, L., Chiquin, M., et al. (2006). Kinematics of the North AmericanCaribbean-Cocos plates in Central America from new GPS measurements across the Polochic-Motagua fault system. *Geophysical Research Letters*, *33*(19), L19309.

Matias, L. M., Cunha, T., Annunziato, A., Baptista, M. a, & Carrilho, F. (2013). Tsunamigenic earthquakes in the Gulf of Cadiz: Fault model and recurrence. *Natural Hazards and Earth System Science*, *13*(1), 1–13.

Matthews, M. V., Ellsworth, W. L., & Reasenberg, P. A. (2002). A Brownian model for recurrent earthquakes. *Bulletin of the Seismological Society of America*, *92*(6), 2233–2250.

McCaffrey, R. (2008). Global frequency of magnitude 9 earthquakes. *Geology*, *36*(3), 263. https://doi.org/10.1130/G24402A.1.

McGuire, R. (1976). FORTRAN computer program for seismic risk analysis. In Technical report, U.S. Geol. Surv., Open File Rep. No. 76–67.

Murphy, S., Scala, A., Herrero, A., Lorito, S., Festa, G., Trasatti, E., et al. (2016). Shallow slip amplification and enhanced tsunami hazard unravelled by dynamic simulations of mega-thrust earthquakes. *Science Reports*, *6*, 1–12.

NGDC/WDS. (2017). National geophysical data center, world data service, global historical tsunami database, national geophysical data center, NOAA. http://www.ngdc.noaa.gov/hazard/tsu_db.shtml/. Accessed 31 Dec 2017.

Okada, Y. (1985). Surface deformation due to shear and tensile faults in a half-space. *Bulletin of the Seismological Society of America*, *75*(4), 1135–1154.

Okal, E. A., Borrero, J. C., & Synolakis, C. E. (2006). Evaluation of tsunami risk from regional earthquakes at Pisco, Peru. *Bulletin of the Seismological Society of America*, *96*(5), 1634–1648.

Ortiz, M., Fernández Arce, M., & Rojas, W. (2001). Análisis de riesgo de inundación por tsunamis en Puntarenas, Costa Rica. *GEOS*, *21*(2), 108–113.

Parsons, T., & Geist, E. (2009a). Tsunami probability in the Caribbean region. *Pure and Applied Geophysics*, *165*(11–12), 2089–2116.

Parsons, T., & Geist, E. L. (2009b). Is there a basis for preferring characteristic earthquakes over a Gutenberg-Richter distribution in probabilistic earthquake forecasting? *Bulletin of the Seismological Society of America*, *99*(3), 2012–2019.

Protti, M., McNally, K., Pacheco, J., Gonzlez, V., Montero, C., Segura, J., et al. (1995). The March 25, 1990 (Mw = 7.0, ML = 6.8), earthquake at the entrance of the Nicoya Gulf, Costa Rica: Its prior activity, foreshocks, aftershocks, and triggered seismicity. *Journal of Geophysical Research: Solid Earth*, *100*(B10), 20345–20358.

R Core Team. (2014). *R: A Language and environment for statistical computing*. Vienna, Austria: R Foundation for Statistical Computing. http://www.R-project.org/.

Rabinovich, A. B., Candella, R. N., & Thomson, R. E. (2013). The open ocean energy decay of three recent trans-Pacific tsunamis. *Geophysical Research Letters*, *40*, 3157–3162.

Rojas, W., Camacho, E., Marroquin, G., Molina, E., & Benito, M. B. (2013). Evolution of the Earthquake Catalog in Central America. In *Meeting of the Americas, AGU, Mexico. S52A08*, Number AGU Meeting of the Americas.

Rojas, W., Bungum, H., & Lindholm, C. (1993). Historical and recent earthquakes in Central America. *Revista Geologica de America Central*, *16*, 5–22.

Rubinstein, R. Y. & Kroese, D. P. (2008). *Simulation and the Monte Carlo Method* (2nd editio ed.). Wiley.

Salazar, W., Brown, L., Hernández, W., & Guerra, J. (2013). An earthquake catalogue for El Salvador and neighboring Central American countries (1528–2009) and its implication in the seismic Hazard Assessment. *Journal of Civil Engineering and Architecture*, *7*(8), 1018–1045.

Sallarés, V., Flueh, E., Charvis, P., & Bialas, J. (2003). Seismic structure of Cocos and Malpelo Volcanic ridges and implications for hot spot-ridge interaction. *Journal of Geophysical Research*, *108*(B12), 2564. https://doi.org/10.1029/2003JB002431.

Satake, K. (1994). Mechanism of the 1992 Nicaragua tsunami earthquake. *Geophysical Research Letters*, *21*(23), 2519–2522.

Schaefer, A., Daniell, J., & Wenzel, F. (2015). State-of-the-Art in Tsunami Risk Modelling for a global perspective. In *EGU General Assembly Conference Abstracts*, Volume 17 of *EGU General Assembly Conference Abstracts*, pp. 5239.

Scholz, C. H., & Small, C. (1997). The effect of seamount subduction on seismic coupling. *Geology*, *25*, 487–490. https://doi.org/10.1130/0091-7613(1997)025<0487:TEOSSO>2.3.CO;2.

Sørensen, M. B., Spada, M., Babeyko, A., Wiemer, S., & Grünthal, G. (2012). Probabilistic tsunami hazard in the Mediterranean Sea. *Journal of Geophysical Research*, *117*(B1), B01305.

Stein, S., Salditch, L., Brooks, E., Spencer, B., & Campbell, M. (2017). Is the Coast Toast? Exploring Cascadia earthquake probabilities. *GSA Today*, *27*, 6–7.

Stepp, J.C. (1972). Analysis of completeness of the earthquake sample in the Puget Sound area and its effect on statistical estimates of earthquake hazard. In *Proc. of the 1st Int. Conf. on Microzonazion, Seattle*, Volume 2, pp. 897–910.

Stirling, M., & Gerstenberger, M. (2010). Ground motion-based testing of seismic hazard models in New Zealand. *Bulletin of the Seismological Society of America*, *100*(4), 1407–1414.

Thio, H. K., Somerville, P., & Ichinose, G. (2007). Probabilistic analysis of strong ground motion and tsunami hazards in Southeast Asia. *Journal of Earthquake and Tsunami*, *01*(02), 1–19.

USGS (2017). *USGS ComCat catalog*. United States Geological Survey. https://earthquake.usgs.gov/earthquakes/search/. Accessed 20 Jan 2017.

van Stiphout, T., Schorlemmer, D., & Wiemer, S. (2011). The Effect of Uncertainties on Estimates of Background Seismicity Rate. *Bulletin of the Seismological Society of America*, *101*(2), 482–494.

VonHuene, R., Ranero, C. R., & Watts, P. (2004). Tsunamigenic slope failure along the Middle America Trench in two tectonic settings. *Marine Geology*, *203*, 303–317.

Ward, S. N. (2001). Landslide tsunami. *Journal of Geophysical Research*, *106*, 11201–11216.

Ward, S. N., & Asphaug, E. (2000). Asteroid impact tsunami: A probabilistic hazard assessment. *Icarus*, *145*, 64–78.

Wessel, P., Smith, W. H. F., Scharroo, R., Luis, J., & Wobbe, F. (2013). Generic mapping tools: Improved version released. *Eos, Transactions American Geophysical Union*, *94*, 45.

Wiemer, S., Giardini, D., Fäh, D., Deichmann, N., & Sellami, S. (2008). Probabilistic seismic hazard assessment of Switzerland: Best estimates and uncertainties. *Journal of Seismology*, *13*(4), 449–478.

Ye, L., Lay, T., & Kanamori, H. (2013). Large earthquake rupture process variations on the Middle America megathrust. *Earth and Planetary Science Letters*, *381*, 147–155. https://doi.org/10.1016/j.epsl.2013.08.042.

Zamora, N. (2016). *Probabilistic tsunami hazard analysis for Central America with focus on uncertainties*. Phd dissertation, Postdam University.

Zamora, N., & Babeyko, A. Y. (2015). Tsunami potential from local seismic sources along the southern Middle America Trench. *Natural Hazards*, *80*(2), 901–934. https://doi.org/10.1007/s11069-015-2004-3.

(Received December 31, 2018, revised October 4, 2019, accepted November 14, 2019)